CHARACTERIZATION OF THE PARTICLE SIZE DISTRIBUTION, MINERALOGY AND FE MODE OF OCCURRENCE OF DUST-EMITTING SEDIMENTS FROM THE MOJAVE DESERT, CALIFORNIA, USA

Adolfo González-Romero[1,2,3], Cristina González-Flórez[1,3], Agnesh Panta[4], Jesús Yus-Díez[5], Patricia Córdoba[2], Andres Alastuey[2], Natalia Moreno[2], Melani Hernández-Chiriboga[1], Konrad Kandler[4], Martina Klose[6], Roger N. Clark[7], Bethany L. Ehlmann[8], Rebecca N. Greenberger[8], Abigail M. Keebler[8], Phil Brodrick[9], Robert Green[9], Paul Ginoux[10], Xavier Querol[2], Carlos Pérez García-Pando[1,11]

[1] Barcelona Supercomputing Center (BSC), Barcelona, Spain
[2] Spanish Research Council, Institute of Environmental Assessment and water Research (IDAEA-CSIC), Barcelona, Spain
[3] Polytechnical University of Catalonia (UPC), Barcelona, Spain
[4] Institute of Applied Geosciences, Technical University Darmstadt, Darmstadt, Germany
[5] Centre for Atmospheric Research, University of Nova Gorica, Ajdovščina, Slovenia.
[6] Karlsruhe Institute of Technology (KIT), Institute of Meteorology and Climate Research Troposphere Research (IMKTRO), Karlsruhe, Germany
[7] PSI Planetary Science Institute, Tucson, AZ, USA
[8] California Institute of Technology, Division of Geological and Planetary Sciences, Pasadena, CA, USA
[9] Jet Propulsion Laboratory, California Institute of Technology
[10] NOAA Geophysical Fluid Dynamics Laboratory, Princeton, NJ, USA
[11] Catalan Institution for Research and Advanced Studies (ICREA), Barcelona, Spain

Corresponding author: Adolfo González-Romero (agonzal3@bsc.es) and Xavier Querol (xavier.querol@idaea.csic.es)

Abstract

Constraining dust models to understand and quantify the effect of dust upon climate and ecosystems requires comprehensive analyses of the physiochemical properties of dust-emitting sediments in arid regions. Following previous studies in the Moroccan Sahara and Iceland, here we analyse a diverse set of crusts and aeolian ripples (n=55) from various potential dust-emitting basins within the Mojave Desert, California, USA. We focus on the characterization of their particle size distribution (PSD), mineralogy, aggregation/cohesion state and Fe mode of occurrence. Our results show differences in fully and minimally dispersed PSDs, with crusts average median diameters (92 and 37 µm, respectively) compared to aeolian ripples (226 and 213 µm, respectively). Mineralogical analyses unveiled strong variations between crusts and ripples, with crusts being enriched in phyllosilicates (24 vs 7.8 %), carbonates (6.6 vs 1.1 %), Na-salts (7.3 vs 1.1 %) and zeolites (1.2 and 0.12 %), and ripples being enriched in feldspars (48 vs 37 %), quartz (32 vs 16 %), and gypsum (4.7 vs 3.1 %). The size fractions from crust sediments display a homogeneous mineralogy, while those of aeolian ripples a more heterogeneous one, mostly due to their different particle aggregation. Bulk Fe content analyses indicate higher concentrations in crusts (3.0±1.3 wt %) compared to ripples (1.9±1.1 wt %), with similar proportions in their Fe mode of occurrence: nano Fe-oxides/readily exchangeable Fe represent ~1.6 %, hematite/goethite ~15 %, magnetite/maghemite ~2.0 % and structural Fe in silicates ~80 % of the total Fe. We identified segregation patterns in PSD and mineralogy differences in Na-salts content within the Mojave basins, that can be explained by sediment transportation dynamics and precipitates due to groundwater table fluctuations described in previous studies in the region. Mojave Desert crusts show similarities with previously sampled crusts in the Moroccan Sahara for PSD and readily exchangeable Fe, yet exhibit substantial differences in mineralogical composition, which should significantly influence the emitted dust particle characteristics.

Keywords: Arid regions, dust sources, desert dust, dust-emitting sediment formation model, dust mineralogy.

1. Introduction

Desert dust produced by wind erosion of arid and semi-arid surfaces has significant effects on climate and ecosystems (Weaver et al., 2002; Goudie & Middleton, 2006; Sullivan et al., 2007; Crumeyrolle et al., 2008; De Longeville et al., 2010; Karanasiou et al., 2012; Pérez García-Pando et al., 2014; among others). Dust affects the energy and water cycles through its absorption and scattering of both shortwave (SW) and longwave (LW) radiation (Perez et al., 2006; Miller et al., 2014), and exerts influence on cloud formation, precipitation patterns, and the associated indirect radiative forcing by serving as nuclei for liquid and ice clouds (e.g. Harrison et al., 2019). Dust also undergoes heterogeneous chemical reactions in the atmosphere that enhance their hygroscopicity and modify their optical properties (Bauer et al., 2005), and when deposited into ocean waters, its bioavailable iron content acts as a catalyst for photosynthesis by ocean phytoplankton, thereby increasing carbon dioxide uptake and influencing the global carbon cycle (Jickells et al., 2005).Dust primarily originates from arid inland basins, which include various sedimentary environments such as aeolian deposits, endorheic depressions, and fluvial- and alluvial-dominated systems (Bullard et al., 2011). Wind typically mobilizes loose sand from adjacent ripples or dunes, which then erodes more consolidated surfaces, typically paved sediments and crusts, to release dust (Stout and Lee, 2003; Shao et al., 2011). Atmospheric dust emission models have improved by identifying preferential dust sources using criteria like topography and hydrology (Ginoux et al., 2001). However, these models still struggle with capturing small-scale variability partly due to the lack of relevant soil measurements in arid regions, despite advancements in understanding the geomorphological and sedimentological factors influencing dust emissions (Bullard et al., 2011). For instance, the particle size distribution (PSD) and cohesion of the sediments affect saltation bombardment and aggregate disintegration processes involved in dust emission (Shao et al., 1993).

Understanding the mineral composition of dust is also crucial for assessing its climate impact. Dust contains various minerals such as quartz, clay minerals, feldspars, carbonates, salts, and iron oxides. The climate effects of dust are influenced by these minerals' relative abundances, sizes, shapes, and mixing states. For example, iron oxides control solar radiation absorption by dust (Formenti et al., 2014; Engelbrecht et al., 2016; Di Biagio et al., 2019; Zubko et al., 2019), nano Fe oxides and easily exchangeable Fe increase the fertilising effect of dust in ocean and terrestrial ecosystems (Hettiarachchi et al., 2019; Baldo et al., 2020, Hettiarachchi et al., 2020), K-feldspar and quartz impact ice nucleation in clouds (Atkinson et al., 2013; Harrison et al., 2019; Chatziparaschos et al., 2023), and calcite influences acid reactions on dust surfaces (Paulot et al., 2016). The mineralogical composition of dust can vary significantly across different regions due to geological and climatic factors (Claquin et al., 1999; Journet et al., 2014). However, most models assume a globally uniform dust composition due to limited global data on parent soil sources. Only a few models account for dust mineralogical composition variations (e.g., Scanza et al., 2015; Perlwitz et al., 2015; Li et al., 2021; Gonçalves Ageitos et al., 2023; Obiso et al., 2024) by using global soil type atlases and extrapolating from a limited number of analyses (Claquin et al., 1999; Journet et al., 2014). These atlases rely on assumptions about soil texture and color, often base their data on soil samples taken from depths deeper than those relevant to wind erosion, and the method used to characterize particle size and associated mineralogy fully breaks down natural soil aggregates.

Since 2022, the EMIT mission has been acquiring comprehensive measurements of surface mineralogical composition for use in Earth System models (Green et al., 2020). EMIT employs imaging spectroscopy across the visible to short wavelength infrared (VSWIR) spectral range from the International Space Station to map the occurrence and estimate the abundance of ten key dust source minerals. Additionally, EMIT has the potential to estimate surface soil texture. While identifying dominant surface minerals has traditionally been a strength of spectrometers, quantifying these minerals poses significant challenges. Factors such as mineral grain size and composition can affect spectral absorptions, certain dominant materials like quartz and feldspar exhibit minimal absorption features, and the presence of other materials can further complicate the analysis.

Overall, there is a notable lack of comprehensive measurements characterizing relevant properties of surface sediments in dust source regions. This gap hampers our ability to evaluate and constrain mineral abundance derived from reflectance spectroscopy and to improve dust emission modeling. Addressing this issue, the FRontiers in dust minerAloGical coMposition and its Effects upoN climaTe (FRAGMENT) project has, over recent years, conducted a series of coordinated and interdisciplinary field campaigns across remote dust source regions. The project's objectives include enhancing the understanding and quantification of dust-source properties, examining their relationship with emitted dust characteristics, refining spaceborne spectroscopy retrievals of surface minerals (Green et al., 2020, Clark et al., 2024), and improving the representation of dust mineralogy in Earth system models (Perlwitz et al., 2015; Li et al., 2021; Gonçalves et al., 2023; Obiso et al., 2023). The FRAGMENT field campaigns involved regional sediment sampling in several regions and detailed wind erosion and dust emission measurements at selected sites. Studies stemming from these activities include those by González-Romero et al. (2023), González-Flórez et al. (2022), and Panta et al. (2022), and González-Romero et al. (2024). These campaigns have been executed in various geographic locations, such as the Moroccan Sahara (2019), Iceland (2021), the Mojave Desert in the United States (2022), and Jordan (2022). Through these efforts, the FRAGMENT project contributes to filling critical knowledge gaps in dust-source characterization.

Following our previous studies in the Moroccan Sahara (González-Romero et al. 2023) and Iceland González-Romero et al. (2024), this study focuses on the characterization of dust-emitting sediments collected from the Mojave Desert in 2022. The Mojave Desert is a closed-basin wedge-shaped region located in the southwestern United States, between California and Nevada. The region is surrounded by mountain ranges and traversed by the Mojave river and other intermittent rivers for over 200 km from the San Bernardino mountains to the east (Dibblee, 1967, Reheis et al., 2012). Despite its limited global importance (dust emission from North America represents only ~3 % of the global dust emission; Kok et al., 2021), the Mojave Desert is an important regional dust source (Ginoux et al., 2012), with most emission occurring in the playa lakes and alluvium deposits near playa lakes (Reheis & Kihl, 1995; Reheis et al. 2009, Urban et al., 2018). Reynolds et al. (2009) observed 71 days with dust plumes during 37 months of camera recording at the Franklin Lake playa. According to remote sensing data (MODIS), aerosol optical depth (AOD) is higher in spring and summer and reaches a minimum in winter (Frank et al., 2007). However, from November to May, eastward flows of the jet-stream affect the Mojave Desert, which, in combination with topography, favour the development of northerly winds that can lead to dust emission (Urban et al., 2009). Up to 65 % of emission in the Mojave Desert is estimated to be due to natural factors, whereas 35 % to anthropogenic activities, including off-road recreation practices, mine operations, and military training and livestock grazing (Frank et al., 2007). The AOD in this region is also affected by dust transported from other regions (Tong et al., 2012) and pollution transported from the Los Angeles Basin (Frank et al., 2007, Urban et al., 2009). In the Mojave

Desert, Reynolds et al. (2009) noted an association between wet periods and dust emission, directly related to the generation of new thin crusts and salt crust removal.

The Mojave Desert includes several significant playa lakes, such as Rogers and Rosemond, Owens Lake, Death-Valley-Badwater, Panamint Valley, Bristol, Cadiz and Danby, Searles Lake, Soda Lake, and Mesquite Lake, among others (Reheis & Kihl, 1995; Reheis, 1997; Potter and Coppernoll-Houston, 2019). Reynolds et al. (2007 and 2009) distinguished between two types of playa lakes: wet playas influenced by groundwater, and dry playas, unaffected by groundwater, though both can experience surface-water runoff. Goudie (2018) further delineated wet playas as having a groundwater table within 5 m of the surface, while dry playas have a groundwater table deeper than 5 m. Additionally, Goudie (2018), Buck et al. (2011), Nield et al. (2015) and Nield et al. (2016) observed that the interaction between salt minerals and the groundwater table on wet playas lead to the formation of fluffy surfaces through salt reworking by water during evapotranspiration.

In the Mojave Desert, three different Aridisols are present in the Rand mountains alluvial fan, corresponding to Xerillic soils or Aridisols according to Eghbal & Southard (1993), typical in arid and semi-arid regions, with low organic matter content and low structures. The uppermost layer of those Aridisols, ranging from 0 to 1 cm in depth exhibited a texture of 15-30% gravel, 69-74 % sand and 10-11 % clay. Reheis et al. (1995) described soils (<2 mm) primarily composed of silt (30-70 %) and clay (20-45 %). The mineralogy of those samples was dominated by quartz, feldspars, amphiboles, and clay minerals, including smectite, mica and kaolinite (Eghbal & Southard, 1993). The Cronese Lakes and Soda Lake playas are documented to contain salt precipitates, but mineralogy is not specified. Mesquite Lake playa is noted for its gypsum deposits (Reynolds et al., 2009). At Franklin Lake playa, surfaces are characterized by silt-clay size particles (Goldstein et al., 2017) with mineralogical descriptions provided in Reynolds et al. (2009) indicating fluffy surfaces comprised of halite, thenardite, trona, burkeite, calcite, illite, smectite, and kaolinite. Similar mineralogical results are described at Soda Lake by Reheis et al. (2009), with a higher proportion of Na-salts, quartz, gypsum and carbonates. Furthermore, Goldstein et al. (2017) identified a diverse array of minerals at Franklin Lake playa, including clays, zeolites, plagioclase, K-feldspar, quartz, calcite, dolomite and salt minerals such as trona, halite, burkeite and thenardite.

This study characterises the particle size distribution, mineralogy and modes of occurrence of Fe of selected potential dust-emitting sediment surfaces from the Mojave Desert. In addition, the mineralogy of different size fractions is analysed, based on a sieving protocol that minimally disturbs sediments. We further discuss the potential effect of sedimentary transport on the particle size and mineralogy across the sampled basins building upon previous studies in the literature. Finally, our results are broadly compared with current EMIT standard (semi-quantitative) products, and with those obtained using similar protocols in previous FRAGMENT campaigns in other regions (González-Romero et al., 2023; González-Romero et al., 2024).

2. Methodology

2.1 Study area

The Mojave Desert, located between California and Nevada, has a diverse geological history spanning from the Cambrian and Precambrian eras to the Holocene (Figure 1). This geological complexity encompasses volcanic, plutonic, metamorphic, and sedimentary units (Jennings et al., 1962; Miller et al., 2014). In areas once submerged during the last glacial maximum (LGM), we now find ephemeral playa lakes that have existed for thousands of years since the LGM, offering a glimpse into the region's dynamic past (Miller et al., 2018). These playa lakes together with alluvial fans, floodplains and other features are surrounded by a variety of source rocks, exhibit diverse particle sizes and compositions and can potentially emit dust under favourable wind conditions.

The regional distribution of the annual Frequency of Occurrence (FoO) of dust events, with dust optical depth exceeding 0.1, derived from MODIS Deep Blue C6.1 Level 2 data following the methodology of Ginoux et al. (2012), is illustrated in Figure 2. The FoO provides an overall estimate of dust emission frequency above a certain threshold at a resolution of 0.1º by 0.1º over the region. Sediment samples were collected from various locations within the Mojave Desert region, including areas with relatively high FoO (see locations in Figures 1 and 2). Among these locations is Soda Lake and its surroundings, near Baker, CA, which is linked to Silver Lake to the north and is surrounded by igneous, volcanic, and carbonate rocks, as well as dune fields to the south (Figure 1). The area is influenced by aeolian, alluvial, and fluvial processes and experiences annual precipitation of 80-100 mm (Urban et al., 2018). This ephemeral lake contains salts resulting from the evaporation of groundwater sourced from an aquifer nestled in the Zzyzx Mountains (Honke et al., 2019). Dust emissions are a recurrent phenomenon, originating from fine sediments accumulated in the lake’s central areas during sporadic floodings, from the white evaporite surfaces in the lake, and from the alluvial deposits to the south of the playa lake (Urban et al., 2018). According to the FoO, the areas with higher dust emissions are the southern part of the lake and the alluvial deposits to the southwest, extending up to Afton Canyon.

Samples were also collected from the Cronese lakes, Mesquite Lake, Ivanpah Lake and Coyote Lake (Figure 1), which lie in areas with significant FoO signals (Figure 2) and have been documented as dust sources in Reheis & Kihl (1995) and Reheis et al. (2009). The Cronese lakes are adjacent to the Soda Lake area to the west, sharing a similar geologic context (Figures 1 and 2). Mesquite Lake, located on the border between California and Nevada, is encircled by carbonate and igneous rocks, mirroring the geological setting of the nearby Ivanpah Lake. Notably, Mesquite Lake playa is the only playa affected by a gypsum mine pit, as documented by Reynolds et al. (2009). Further contributing to the diversity of the region's geological makeup is Coyote Lake, flanked by Miocene and Pleistocene sediments. These playa lakes, characterized as endorheic ephemeral lakes, receive groundwater inputs in some cases, enriching the lakes with salts that subsequently precipitate on the surfaces of their central regions (Whitney et al., 2015; Urban et al., 2018).

Other areas with relatively high FoO not sampled in our study include the Ashford Junction alluvial deposits and the Fort Irwin area, where the northern valley, including Nelson Lake, may be more prone to dust emission due to significant anthropogenic disturbance. It is important to note that the FoO may tend to highlight areas such as playas and their surroundings, where in some cases the most dust per unit area could be produced (Floyd and Gill, 2011; Baddock et al., 2016). However, some alluvial regions with lower emission rates not surpassing the FoO threshold may produce more dust overall due to their greater areal extent (Reheis and Kihl, 1995; Baddock et al., 2016). Additionally, many other types of dust-producing surfaces active in the Mojave Desert, such as gravel roads, agricultural lands, and recreational off-road tracks, are rarely observed by satellite retrievals (Urban et al., 2018).

The new EMIT sensor onboard the International Space Station offers a glimpse of the mineralogical diversity in the Mojave Desert (Green et al., 2020). Figure 3 displays standard Tetracorder RGB color composite semi-quantitative products for EMIT. Tetracorder is a software system that employs a set of algorithms within an expert system decision-making framework to identify and map compounds (Clark, 2024; Clark et al., 2024). Figure 3 shows a true color image, along with standard products for Fe^{2+} and Fe^{3+} bearing mineral electronic absorptions (including hematite and goethite) in the visible to very-near infrared spectral range. It also displays standard products for the EMIT-targeted minerals, excluding hematite and goethite: calcite, chlorite/serpentine, dolomite, gypsum, illite/muscovite, kaolinite-dioctahedral group, montmorillonite group, and vermiculite. These products highlight areas where the presence of each mineral or component is significant, measured in terms of band depth*fit, where the fit represents the least squares correlation coefficient from a feature fit of observed and reference library spectra. These analyses reveal the widespread presence of phyllosilicates such as kaolinite, smectite, montmorillonite, and illite across the area. The northeastern sector, particularly around Mesquite Lake, exhibits notable concentrations of carbonates and gypsum. Additionally, goethite and hematite are detected, with a more pronounced presence of goethite in the northern portion and hematite in the southern part of the region. The detection of mixtures of Fe^{2+} and Fe^{3+} within various minerals enriches our understanding of the region's mineralogical diversity.

Quantitative surface mineralogy (mineral mass abundances of the 10 EMIT-targeted minerals) and soil texture products are currently being developed by the EMIT team for use in Earth System Models. Their publication and evaluation will be the focus of forthcoming publications. Thus, it is beyond the scope of this study to perform a detailed quantitative comparison between our analyses and comparable EMIT products. However, in the results section, we broadly compare these standard products with the results of our in-situ analyses.

2.2 Sampling

Representative surfaces of dust-emitting sediments were sampled in May 2022, with depths of up to 3 cm, using a 5 cm2 inox shovel. Samples were stored in a plastic bag, labelled, and documented with photographs, descriptions, and coordinates, and transported to the laboratories for subsequent analyses. The type of samples considered are crusts (semi-cohesive fine sediments accumulated during floodings in depressions) and ripples (aeolian ripples that are built up under favourable winds and supply sand for saltation) (Figure 4). A total of 55 surface sediments and ripples (32 from Soda Lake, 9 from Mesquite Lake, 1 from Ivanpah Lake, 11 from the Cronese Lakes, and 2 from Coyote Lake) were sampled for laboratory analysis. Once in the laboratory, the samples were dried for 24-48 h at 40-50 ºC, sieved to pass through a 2 mm mesh.

Our rationale for selecting crusts and ripples is two-fold. On the one side, dust emission is primarily driven by two mechanisms: saltation bombardment and aggregate disintegration. In saltation bombardment, dust is ejected from soil aggregates (typically crusts and paved sediments rich in clay and silt particles) when impacted by saltating sand particles. In aggregate disintegration, dust is released from saltating soil aggregates (Shao et al., 1993; Alfaro et al., 1997; Shao, 2001). By characterizing the PSD (both dry and wet sieved) and mineralogy of ripples (concentrating sand particles) and crusts (concentrating clay and silt particles), we provide comprehensive and valuable information for developing and refining dust emission models. On the other side, in arid regions, quartz and feldspar typically dominate sediment mass. However, current spaceborne hyperspectral instruments (such as EMIT) cannot directly identify feldspar and quartz because their absorption features lie outside the instrument's spectral range. This poses a significant challenge in quantifying surface mineral abundances from remote spectroscopy. At all FRAGMENT sampling locations (Morocco, Iceland, US-Mojave, and Jordan), we measured reflectance spectra using an ASD Fieldspec 3. By characterizing and contrasting ripples (with high quartz and feldspar content and larger particle sizes) and crusts, we aim to provide information to enhance understanding and improve modelling assumptions for estimating surface mineral abundances and soil texture from remote spectroscopy in subsequent studies.

We acknowledge that the limited number of samples collected may not fully represent the potential variability among crusts and ripples within the studied locations due to varying conditions (Buck et al., 2011). However, our samples broadly represent the composition and particle size distributions (PSDs) of this type of sediments in these areas, allowing for meaningful comparisons with sediments from other locations.

2.3 Analyses

2.3.1 Particle size distribution

Particle size distributions (PSD) of bulk samples (<2 mm) were analysed as described in González-Romero et al. (2023) for the evaluation of the aggregation state. First, we conducted a minimally dispersed PSD (MDPSD) analysis, which minimizes the breaking of the aggregates that are encountered in natural conditions. Second, we conducted a fully dispersed PSD (FDPSD) analysis, which breaks the aggregates. Wet dispersion was done according to Sperazza et al., (2004), using water and sodium hexametaphosphate dispersion for 24 h. Both PSDs (MDPSD and FDPSD) were obtained by a laser diffractometer with the Malvern Mastersizer 2000 Hydro G and Scirocco for the fully and minimally dispersed conditions, respectively. We note that under wet dispersion, at least some salt minerals may dissolve.

In addition, we separated 20 selected samples from different sources, including 16 crusts and 4 aeolian ripples, into different size ranges to understand how mineral composition changes with size. We used a series of sieves with mesh sizes of 2 mm, 1 mm, 500 µm, 250 µm, 80 µm, 63 µm, 40 µm, and 20 µm. The sieving process involved hand shaking the full column for 1 minute, followed by ultrasound sonication for 1 minute at the 500 µm, 80 µm, 40 µm, and 20 µm size fractions. This method ensured the effective separation of the size fractions for subsequent mineralogical analysis.

2.3.2 Mineralogical composition

To quantify the different contents of crystalline minerals and amorphous components, X-Ray Diffraction (XRD) coupled with a Rietveld quantitative method were used (Rietveld, 1969; Cheary and Coelho, 1992; Young, 1995 and Topas, 2018). Adding a known amount of an internal standard material allowed, via the Rietveld method, the quantification of a mixture of minerals and any non-crystalline material in the mixture not included in the Rietveld method (De la Torre et al., 2001; Madsen, 2001, Scarlett and Madsen, 2006; Machiels et al., 2010; Ibañez et al., 2013). For the analysis, a measured amount of dry ground sample was mixed and dry ground again with 10-20 % of fluorite (CaF_2 powder, Merck), used here as an internal standard for quantitative purposes. The XRD patterns of the samples were analysed by a Bruker D8 A25 Advanced Powder X-ray diffractometer operated at 40kV and 40 mA with monochromatic Cu Kα radiation (=1,5405 Å). This device uses a Bragg-Brentano geometry and a sensitive detector LynxEye 1D. Diffractograms were recorded from 4 to 120º of 2θ and steps of 0.015º in 1s and maintained rotation (15/min). For the clay identification, samples were analysed using the oriented aggregate method by XRD, decanting clay fractions from samples and smearing the slurries in glass slides. After, three treatments were applied including air drying (AO), glycolation with ethylene glycol (AG) and heating at 550 ºC for 2h (AC) with its three different diffractograms. Finally, the three diffractograms allows to corroborate the presence of Illite, Chlorite, Palygorskite and Montmorillonite through Thorez (1976) and USGS Open File procedures. Data collected were evaluated using the Bruker AXS DIFFRAC.EVA software package (Bruker AXS, Karlsruhe, Germany, 2000) and the Rietveld analyses performed with TOPAS 4.2 program (Bruker AXS, 2003-2009). A Chebyshev function of level 5 was used to fit the background and abundances of crystalline phases and amorphous phases were normalised to 100 wt %. Fits were evaluated by visual comparison, the R_{wp} (R-weighted pattern), R_{exp} (R-expected), and Goodness of Fit (GOF).

2.3.3 Mode of occurrence of Fe

As XRD is not precise enough for Fe-oxide quantification, wet chemistry and sequential extractions of Fe are needed for quantification of the mode of occurrence of Fe (González-Romero et al., 2023; 2024). Samples were analysed with a two-step acid digestion for the total Fe (FeT) content following the procedure by Querol et al. (1993, 1997). A reference material (NIST-1633b, coal fly ash) was used for quality control in every batch. The sequential extraction presented in Shi et al. (2009), Baldo et al. (2020) and González-Romero et al. (2024) were used to quantify readily exchangeable Fe ions and nano Fe oxides (FeA), the amount of crystalline Fe oxides as goethite and hematite (FeD), and crystalline magnetite (FeM). For the 1st extraction, 30 mg sample were leached with 10 ml of an ascorbate solution (extractant solution) and shaken in dark conditions for 24 h and filtered. Another 30 mg were leached with 10 ml of a dithionite solution (extractant solution), shaken for 2 h in dark conditions and filtered for the 2nd extraction. The solid residue was then leached again in 10 ml of an oxalate solution for 6 h in dark conditions and filtered for the 3rd extraction. The extracted solution of each phase (FeT, FeA, FeD and FeM) was analysed to quantify dissolved Fe by Inductively Coupled Plasma Atomic Emission Spectrometry (ICP-AES). FeA is obtained with the 1st extraction, FeD is obtained subtracting from the 2nd extraction the amount of Fe from the 1st extraction. Finally, the FeM is related to the 3rd extraction. At the end, the equivalent to the Fe as structural Fe was obtained: FeS = FeT - FeA - FeD - FeM which is included in other minerals and amorphous phases. To test accuracy, 30 mg of Arizona Test Dust (ATD; ISO 12103-1, A1 Ultrafine Test Dust; Powder Technology Inc.) was subjected to the same extraction procedure in every batch and extraction.

The averaged Fe content of the reference material 1633b was 7.6 ± 0.5 % (certified 7.8%). Furthermore, the average values of the sequential Fe extraction of the ATD reference material were 0.073 ± 0.012, 0.47 ± 0.01, and 0.042 ± 0.002 % for FeA, FeA+FeD and FeM, respectively, while the certified contents are 0.067, 0.48, and 0.047 %, respectively.

3. Results

3.1. Particle size distribution

The PSD and median particle diameter of fully and minimally disturbed samples are key parameters for understanding the cohesion and aggregation state of sediments (González-Romero et al., 2024). We note that in the Mojave Desert some basins are enriched in salts, which can cause some artefacts in the FDPSD. The dissolution of salts during wet dispersion for bulk PSD analysis (<2 mm) can remove aggregating agents. These salt cementation of the crusts might reduce the dust emission potential of the surface.

The average PSDs of crusts across different basins exhibit remarkable similarity, yet disparities between FDPSDs and MDPSDs are pronounced, indicating varying degrees of particle cohesion and aggregation at Cronese, Mesquite, Ivanpah and Coyote lakes. In these locations, FDPSDs feature a dominant mode at 8-10 µm alongside a coarser mode at 100 µm, while MDPSDs are characterized by a dominant coarser mode (Figure 5). In contrast, Soda Lake crusts exhibit similarity between FDPSDs and MDPSDs. Averaged FDPSDs and MDPSDs of aeolian ripples from the Mojave Desert are found to be similar, typically featuring a major size mode between 100-300 µm. However, distinctions arise when analysing specific lakes. Aeolian ripples from Soda, Cronese, and Coyote lakes showcase a dominant coarse mode at 200-300 µm, whereas those from Mesquite Lake show a dominant mode at a finer scale, approximately at 100 µm (Figure 5).

The crusts' mean of all median particle diameters (mean median) in the analyzed Mojave Desert dust source sediments reveal a coarser MDPSD compared to FDPSD, with values of 92 and 37 µm, respectively. In contrast, the mean median particle diameter is similar for aeolian ripples (226 and 213 µm, respectively) (Table S1). Analysing specific locations, the mean median particle diameter from the MDPSD of crusts varies, with the finest crust observed at Ivanpah Lake (35 µm) and the coarsest at Mesquite Lake (141 µm). For FDPSD, the finest crust originates from Coyote Lake (8.4 µm), while the coarsest is from Soda Lake (52 µm) (Table S1). Similarly, for aeolian ripples, the mean median particle diameters for both MDPSD and FDPSD are finer at Mesquite Lake (167 and 67 µm, respectively) and coarser at Cronese lakes (264 and 234 µm, respectively) (Table S1). The high degree of particle aggregation observed in crusts, contrasting with the lower aggregation state in ripples, aligns with findings reported for dust-emitting sediments from Morocco by González-Romero et al. (2023).

The mean median particle diameters of crusts collected in the Mojave Desert are similar to those from the Morocco described by González-Romero et al. (2023). Specifically, the mean median MDPSD diameter for the Mojave Desert (92 ± 74 µm) closely resembles that of the Morocco Draâ Lower basin (113 ± 79 µm), albeit slightly finer, and is notably coarser than that of Iceland (55 ± 62 µm) (González-Romero et al., 2023, 2024). Furthermore, while the finest crust sampled in the Mojave Desert (Ivanpah with 35 µm) is almost twice as coarse as the finest from Morocco (L'Bour with 20 µm). For FDPSD, the Icelandic top sediment surface is the coarsest (56 ± 69 µm), followed by both Morocco and Mojave crusts (37 ± 77 and 37 ± 48 µm, respectively). Additionally, average MDPSD median diameters of aeolian ripples from the Mojave Desert sources samples closely resemble those from Morocco (226 and 221 µm, respectively), while those from Iceland are slightly coarser (280 µm).

Dry sieved size fractions of dust-emitting sediments show the highest percentage of mass in the 250-500 and 80-250 µm fractions, with minimal mass at 500-1000 µm and 1-2 mm and in the finer fractions (20-40 and <20 µm) (Figure 6, Table S2). In both cases, the size fractions from 80 to 500 µm accumulated a total of 75 to 90 % of the total mass fraction (Table S2).

Close to the centre of the Soda Lake, where numerous crust samples were collected, before reaching massive crust cementation by evaporite minerals, the FDPSD median diameter reaches very fine sizes (8-15 µm) (Figure S1). In contrast, towards the edges of the basin (closer to the mountains surrounding this endorheic lake), the size markedly increases, ranging from 22 to 87 µm (Figure S1). Similar patterns, yet with coarser sizes, are observed for the MDPSD. As described in previous studies, the fluctuation of the groundwater table in the centre of the basin can lead to a massive precipitation of salts, resulting in the formation of compact crusts (Figure 4) (Reynolds et al., 2007; Nield et al., 2016a; Nield et al., 2016b; Urban et al., 2018) that should effectively reduce dust emission. However, at the edges, where the precipitation of salts is less frequent, and reworking of the crusts by fluctuations in the groundwater occurs, salty and spongy crusts are formed (Figure 4) (Nield et al., 2016a and Nield et al., 2016b). These spongy crusts, being less compact, are more easily broken by saltating particles, potentially leading to high-salt dust emissions.

The slight particle size segregation, with finer particles accumulating towards the center of the lake, can be attributed to the transport of sediments from the surrounding mountains to the lake's center by runoff waters during rain episodes. Initially, the coarser particles are deposited, followed by the finer particles that remain suspended in the water for a longer duration. Nevertheless, the crusts in the surroundings alluvial fans of the Soda Lake (22-87 µm in the edges compared to 8-15 µm in the centre, Figure S1) are fine enough and surrounded by dunes (availability of saltators for saltation bombardment) to have a high potential dust emission under favourable conditions (Reynolds et al., 2006; Reheis et al., 2009; Urban et al., 2018).

3.2. Mineralogy

Dust-emitting sediments from the Mojave Desert primarily consist of feldspars (41 ± 12 %, including albite/anorthite and microcline), quartz (22 ± 11 %) and clay minerals (18 ± 12 %, such as kaolinite, montmorillonite and illite). Additionally, minor contents of carbonate minerals (6.6 ± 6.6 %), amphibole (pargasite) 4.1 ± 1.5 %, and iron oxides (maghemite/magnetite) (0.77 ± 0.54 %) are observed (Figure 7, Tables 2 and S3). At Soda, Mesquite and Cronese lakes, Na-salts such as halite, thenardite, trona, and burkeite are also present, with an average salt content of 5.0 ± 11 %. Additionally, zeolites (0.77 ± 1.1% to 8.5%) including laumontite and analcime are detected at Soda, Cronese, and Coyote lakes (the southern sites), with the highest content observed at Coyote Lake. High amounts of gypsum are found at Mesquite Lake (15 ± 29 %) (Figure 7, Tables 2 and S3). Moreover, Mesquite Lake crusts exhibit high contents of dolomite and calcite (15 ± 11%) compared to other basins (3.6 ± 2.6% to 7.2%) (Table 2).

The overall mineral composition of the dust-emitting sediments originates primarily from the source rocks prevalent in the region. These include dominant of Mesozoic granitic rocks, as well as pre-Tertiary, Tertiary and Quaternary volcanic rocks, and Pre-Cambrian and Mesozoic metamorphic rocks (Figure 1). In the northern, northeastern, and eastern areas of Mesquite Lake, an important limestone and dolostone massif from the Palaeozoic era contributes notably to the high content of calcite and dolomite in the sediments of this lake (Figure 1). Zeolite content in the sediments may be attributed to the weathering of volcanic outcrops in the region or to precipitation in alkaline lakes. This diverse bedrock mineralogy results in a wide variety of minerals in the dust-emitting sediments. The form of iron oxide detected in the samples, identified via XRD, is maghemite. However, distinguishing between maghemite and magnetite using XRD is challenging (Vandenberghe et al., 2000), and magnetite has been found to be ubiquitous in Mojave dust (Reheis et al., 2009; Reynolds et al., 2006). Therefore, we refer hereafter to maghemite/magnetite to account for the potential presence of both minerals in the samples. In comparison to aeolian ripples, the average composition of the crusts shows enrichment in clay minerals (24 ± 11 versus 7.8 ± 2.3 % in crust and ripples, respectively), carbonates (6.6 ± 6.6 versus 1.1 ± 2.2 %), Na-salts (7.3 ± 13 versus 1.1 ± 3.7 %), zeolites (1.2 ± 1.9 versus 0.12 ± 0.52 %) and maghemite/magnetite (0.92 ± 0.59 versus 0.49 ± 0.28 %), while being depleted in quartz (16 ± 7.2 versus 32 ± 9.5 %), feldspars (37 ± 9.7 versus 48 ± 13 %) and gypsum (3.1 ± 14 versus 4.7 ± 20 %), with similar amphibole content (4.1 ± 1.5 versus 4.1 ± 1.6 %) (Figure 7, Tables 2 and S3). These mineral enrichment and depletion trends in crusts are observed in all the playa lakes, except for Mesquite Lake, which is discussed below.

In Soda Lake, the concentration of Na-salts in crusts increases towards the inner part of the lake, ranging from 5-10 % at the margins to 45-50 % in the centre, where compact and fully salt-cemented crusts form. This phenomenon is illustrated in Figure 8, which presents a geological and mineralogical cross-section of Soda Lake. In addition to the water transport to this central part of the basin during the rain episodes, groundwater discharge from the Zzyzx mountains occurs. There, the groundwater table is close to the surface, and its interaction with the surface causes the massive mobilisation of Na-salts that consolidate the crusts (Figure 4) (Nield et al., 2016b). Cycles of precipitation and dissolution of the salts yield salty spongy crusts (Figure 4) at the edges of these massive crusts, with higher dust emission potential in the degraded salty crusts (Nield et al., 2016a). The very high content of Na-salts content in Soda Lake is attributed to the continuous high Na-S-Cl groundwater interaction in the vicinity of Zzyzx, defining Soda Lake as a wet playa lake according to Reynolds et al. (2009) and Urban et al. (2018). On the other hand, Cronese, Coyote, and Ivanpah are categorized as dry lakes.

Mesquite Lake features extensive gypsum deposits at the surface, which are a major component of both dunes and crusts. A small gypsum mine operates in Mesquite Lake. The gypsum content in crusts is notably higher at the center (80%) compared to the margins (3-11%). In contrast, the contents of Na-salts and carbonates are greater at the margins (30% and 12-18%, respectively) than at the center (7.5-14% and <0.1-6.9%, respectively). Aeolian ripples at the center of Mesquite Lake exhibit a very high gypsum content, whereas at the margins, these ripples contain higher amounts of quartz, feldspars, and clays than at the center. Despite the presence of the disturbed mine area, most large dust events at Mesquite Lake have been observed to originate from natural (undisturbed) playa surfaces near the margins (Reynolds R., personal communication).

Amphiboles in the Mojave Desert, sourced from metamorphic rocks of the area, are homogeneous and can serve as a marker for emitted desert dust in the region. Comparing mineralogy from Mojave Desert crusts to Moroccan surface samples (González-Romero et al., 2023), the former are largely enriched in feldspars, clay minerals, Na-salts, and gypsum, and depleted in quartz and carbonates, with trace proportions of amphibole, zeolites, and maghemite/magnetite. Ripples in the Mojave Desert are depleted in quartz and carbonates, enriched in feldspars, clay minerals, Na-salts, and gypsum, with traces of amphibole, maghemite/magnetite, and zeolites compared to Moroccan ripples. The mineralogy of the Mojave Desert is markedly different from that of Iceland, due to differences in bedrock geology, although both contain feldspars, zeolites, and maghemite/magnetite (González-Romero et al., 2024).

Particle aggregation of the dust-emitting sediments from the Mojave Desert samples is similar to those described by González-Romero et al. (2023) for Moroccan samples, likely due to the presence of clays, Na-salts and precipitated carbonates. This aggregation inhibits aerodynamic entrainment and dust emission should be primarily controlled by saltation bombardment (Shao et al., 1993). According to the XRD analysis, the occurrence of crystalline Fe oxides is limited to maghemite/magnetite in contrast to the hematite/goethite content found in Moroccan crusts (González-Romero et al., 2023). However, due to the XRD low precision on the detection of low contents of minerals such as hematite and goethite, their presence in the samples cannot be ruled out. In fact, both the EMIT standard products (Figure 3), and the Fe mode of occurrence analysis discussed in the next section suggest the presence of hematite and goethite.

The EMIT standard products (Figure 3) indicate the presence of phyllosilicates such as kaolinite, smectite, montmorillonite, and illite, broadly consistent with our results. Specifically, around Mesquite Lake, where elevated levels of gypsum and carbonates were detected, the EMIT results corroborate the significance of these minerals in the same vicinity. Similarly, in Coyote, Ivanpah, and Cronese Lakes, there is agreement regarding the prevalence of illite and muscovite as the major clay minerals, alongside kaolinite. However, discrepancies arise in Soda Lake, where EMIT identifies a dominant presence of montmorillonite, contrasting with our XRD results indicating a predominance of illite, muscovite, and kaolinite. While Tetracorder identified predominant montmorillonite, illite, muscovite and kaolinite could be on the order of 30% of the montmorillonite abundance and not show in the EMIT spectra without a more sophisticated non-linear radiative transfer model to find the relative abundances of these two minerals. This is due to the relative absorption strengths of the spectral features of these minerals relative to those in montmorillonite While our XRD analyses highlight the presence of maghemite/magnetite, these minerals do not present clear absorbing features in the spectral range of the EMIT instrument and are not considered within the 10 EMIT standard minerals. In contrast to the XRD results, EMIT highlights the significant presence of goethite in the northern sources (Mesquite and Ivanpah Lakes). Conversely, in the southern sources (Soda, Cronese, and Coyote Lakes), EMIT highlights a major mixture of Fe2+ and Fe3+ species. The limited precision of XRD for low proportions of Fe oxides, underscores the need for complementary techniques and analyses to bolster our findings.

The mineralogical composition of the dry size-segregated fractions of the dust-emitting sediments is outlined in Table S4. The findings indicate that there is no significant size enrichment process in crusts; rather, there exists a relatively uniform distribution of quartz, feldspars, zeolites, and Fe oxides across all size fractions (Figure 6). A slight, albeit not significant, enrichment of carbonates and clays is observed, along with a slight depletion of Na-salts and gypsum in the finer fractions (<20 µm). Additionally, pargasite shows a slight enrichment in the 40-80 µm fraction. In contrast, for aeolian ripples, quartz exhibits significant enrichment in the coarser fraction (250-500 µm) and depletion in the finer ones (<80 µm). Regarding carbonates, clays, and Fe oxides, there is an enrichment towards the finer fractions (<20 µm), while the content of feldspars remains relatively homogeneous. Pargasite content increases in the 40-80 µm fraction, and Na-salts and gypsum are either not detected or present in trace amounts (Figure 6). The notable disparity in the enrichment factor between crusts and aeolian ripples is partly attributed to the reduced amount of sand and the differing cohesion states: crusts exhibit high cohesion, resulting in a homogenized mineralogy across size fractions (as aggregates form a homogeneous concretion of minerals), while aeolian ripples display lower or negligible aggregation, leading to a slightly more heterogeneous mineralogy across size fractions compared to crusts.

3.3. Mode of occurrence of Fe

The average content of FeT in the crusts is 3.0 ± 1.3 wt %, while for aeolian ripples is 1.9 ± 1.1 wt %. Among these crusts, 1.8 ± 0.92 % of the FeT occurs as FeA, 17 ± 7.2 % as FeD, 2.1 ± 1.2 as FeM and 79 ± 8.5 % as FeS (Tables 3 and S5). Aeolian ripples have very similar contents and modes of occurrence of Fe in the analysed samples of the Mojave Desert.

Among the crusts, Ivanpah has the highest FeT content at 4.9 %, followed by Cronese and Coyote lakes (3.7 ± 1.2 % and 3.5 %, respectively), with Soda Lake showing a similar content (3.1 ± 1.2 %). Mesquite has the lowest FeT (1.6 ± 0.53 %), probably due to dilution of detrital Fe-bearing minerals with salts and gypsum. FeS is the dominant mode of occurrence in most lakes, ranging from 68 % (1 sample) at Ivanpah, to 74 ± 3.5 and 74 ± 13 % at Mesquite and Cronese, and to 83 ± 2.8 and 82 % at Soda and Coyote lakes. The FeD is higher at Ivanpah (29 %), Cronese Lakes (21 ± 11 %) and Mesquite Lake (20 ± 2.7 %) than at Soda and Coyote lakes (14 ± 2.5 and 14 %). FeM is higher at Mesquite Lake (3.7 ± 1.2 %), followed by Cronese and Coyote lakes (2.3 ± 1.1 and 2.4 %), and Soda (1.5 ± 0.49 %) and Ivanpah Lakes (0.82 %). Finally, FeA is higher at Cronese Lake (2.4 ± 0.99 %), compared to Coyote, Mesquite, Soda and Ivanpah lakes (1.8, 1.8 ± 0.93, 1.5 ± 0.81 and 1.4 %) (Tables 3 and S5). Crusts are enriched in FeT, FeD and FeA compared to ripples, while ripples are enriched in FeM and FeS (Tables 3 and S5).

Overall, the bulk Fe content in crusts is driven by structural Fe from clays and amphiboles (as deduced from the high correlation shown in Figure 9a), followed by small proportions of hematite and goethite (not detected by XRD), which are clearly higher at the northern lakes Ivanpah and Mesquite lakes (consistent with the highlighted presence of goethite in the EMIT standard products), probably due to the Precambrian and Cambrian metamorphic rocks that supply sediments. Furthermore, the easily exchangeable Fe is also driven by clay minerals (Figure 9b).

Compared to crusts in other arid regions analysed by González-Romero et al. (2023, 2024), the analysed Mojave Desert crusts have similar FeT content than Moroccan crusts but are much lower than the Iceland top sediments (loose surface sediments in Iceland according to González-Romero et al. (2024)) (3.0 ± 1.3, 3.6 ± 0.71 and 9.5 ± 0.39 %, for Mojave, Morocco, and Iceland respectively). The proportion of FeS in FeT is similar to the Icelandic sediments but higher than in Moroccan samples (79 ± 8.5 and 79 ± 6.5 %, and 67 ± 2.4, respectively). The proportion of FeM is clearly lower than that of Iceland, but higher than that of Morocco (2.1 ± 1.2 and 16 ± 5.4 %, for Mojave and Iceland; Morocco proportion is negligible). The FeD proportion is intermediate between Morocco and Iceland (17 ± 7.2, 31 ± 2.3, 3.5 ± 1.5 %, respectively), while the FeA proportion is similar to both Morocco and Iceland crusts (1.8 ± 0.92, 1.3 ± 0.39 and 1.9 ± 0.55 %, respectively) (Figure 10).

4. Discussion and conclusions

The playa lakes sampled within the Mojave Desert can serve as significant dust-emitting sources in the region. Descriptions provided by Urban et al. (2018) and satellite imagery (Figure 2) confirm the presence of desert dust emissions originated from these areas. The lithology, geological/tectonic evolution, and past and current climate conditions collectively contribute to the formation of these dust sources in the Mojave Desert.

Dust-emitting sediments in this region predominantly stem from substratum rocks, comprising mainly granitic and volcanic formations, along with metamorphic Pre-Cambrian, Cambrian, Paleozoic, and Mesozoic rocks. Endorheic basins, shaped by faulting during the Tertiary-Quaternary period, accumulated fine sediments through erosion, transportation, and deposition processes. Wetter conditions prevailing during the Pleistocene epoch led to the formation of deep lakes within the basins, which gradually desiccated as the climate evolved. These arid conditions rendered the playa lakes susceptible to dust emission under specific atmospheric conditions. Notably, a particle size segregation is observed, transitioning from coarser sediments in the proximal alluvial areas towards finer particle crusts within the central regions of the lakes. In the playa lakes, finer sediments accumulate towards the centre of the lakes due to flood events inundating the central areas and ponding, which facilitates the deposition of coarser particles followed by top finer sediment sizes.

According to the conceptual model depicted in Figure 11, the finer dust particle size distributions range from 8.4 to 99 µm inside Soda Lake and 46 to 111 µm outside Soda Lake, underscoring this sedimentation process. Comparisons with conceptual models proposed for other regions, such as those by González-Romero et al. (2023, 2024) for locations in Morocco and Iceland, reveal a similar transport fractionation phenomenon occurring in the Mojave Desert. These crusts, observed within Soda Lake, show enrichment in clay minerals, carbonate minerals, salts, and iron oxides, while experiencing depletion in coarser constituents such as feldspars and quartz.

In the Mojave Desert, there are two distinct types of playa lakes, characterized as wet and dry, depending on the regime of the groundwater table and its relationship with the surface, as described by Reynolds et al. (2007 and 2009), Buck et al. (2011), Nield et al. (2016a and b), Urban et al. (2018) and Goudie (2018). Understanding the groundwater table regime is fundamental in this region due to its profound relation on the porosity of the crust and its consequential impact on mineralogy, including the precipitation and enrichment of salts (Figure 11). This dynamic contrasts sharply with other conceptual models, where the relationship between crust formation and the groundwater table is either minimal or absent entirely. For instance, there is no or little relation between crusts and groundwater table in Morocco, and in Iceland, where the water regime is largely influenced by floodings from glaciers (González-Romero et al., 2023, 2024). In wet playa lakes like Soda Lake, the presence of salty crusts, whether massive or spongy, is significantly pronounced. Conversely, in dry playa lakes such as Ivanpah, Coyote, and Cronese, the relationship of salt crusts is notably less prominent as the proportion of Na-salts is lower (see Figure 11).

At Soda Lake, a hard crust, measuring up to 0.5 meters in thickness (Figure 3), forms through the extensive precipitation of Na-salts, particularly near the Zzyzx area, where a relatively constant mobilisation of salts is due to the water table evaporation or vapour discharge from deeper parts of the sediment towards the surface (Nield et al., 2015, 2016a and b). Along the edges of this massive crusty area, the frequent oscillation of the water table may result in the precipitation and dissolution of salts in lower quantities compared to the centre, leading to the formation of weaker crusts characterized by high porosity. These porous crusts may contribute to an increased dust emission rate compared to the hard salt crusts found in the centre. Dry lakes such as Ivanpah, Cronese, and Coyote do not exhibit the formation of spongy crusts due to the low concentrations of salts. In wet playas, strong dust emission may happen when very strong winds rip off thin crusts exposing the fine-grained sediment beneath including lithogenic and salt mineral particles (Rich Reynolds, personal communication).

Particle aggregation facilitated by diagenetic salts and carbonate minerals is prevalent in the samples dust-emitting sediments of the Mojave Desert, akin to the equivalent sediments found in the Moroccan Sahara. The average grain size of the crusts from both regions is similar, with MDPSD values of 113 ± 79 µm for Morocco and 92 ± 74 µm for the Mojave Desert, and FDPSD values of 37 ± 77 µm and 37 ± 48 µm, respectively. These patterns contrast with the lower aggregation state and finer MDPSD observed in Icelandic dust (55 ± 62 µm) (Table 4).

In terms of mineralogy, crusts from the Mojave Desert are enriched in feldspars, clay minerals, Na-salts, and gypsum, whereas crusts from the Moroccan Sahara are enriched in quartz and carbonates (Table 4). The mineralogy of Icelandic top sediments (loose surface sediments in Iceland according to González-Romero et al. (2024)) differs due to their volcanic origin; however, both the Mojave Desert crusts and Icelandic top sediments contain similar amounts of zeolites. Salt enrichment in the crusts is primarily attributed to interactions with the groundwater table as shown in previous studies (Nield et al. (2016a and b), Urban et al. (2018) and Goudie (2018) (Figure 11).

The total iron content (FeT) remains consistent throughout the samples collected in the Mojave Desert, with slightly higher levels observed in the Ivanpah crust, albeit diluted by the high salt content in the wet playa lake crusts or the elevated gypsum content in the Mesquite Lake. While the total Fe content is comparable between the Mojave Desert and Moroccan Sahara crusts (3.0 and 3.6 wt %, respectively), it is substantially lower than in Icelandic top sediments (9.3 wt %). Exchangeable Fe proportions in FeT are similar among the three environments. The proportion of Fe from hematite and goethite in Mojave Desert crusts fall between those of Moroccan Sahara crusts and Icelandic top sediments (17, 31, and 0.5 wt %, respectively). The proportion of maghemite/magnetite in Mojave Desert crusts is much lower compared to Icelandic top sediments (2.1 and 15 %, respectively). Finally, the proportion of structural Fe in the samples is similar across the three environments.

In conclusion, the dust-emitting sediments collected from the Mojave Desert exhibit distinct signatures in mineralogy and modes of occurrence of Fe compared to those from the Moroccan Sahara, despite similar particle sizes. These differences can influence emitted dust properties, and associated impacts. Similarities in fully disturbed and minimally disturbed particle size distributions support comparable dust emission mechanisms, with saltation bombardment playing a prominent role.

Code availability. The Tetracorder code used in this paper is provided by Clark (2023, https://github.com/PSI-edu/spectroscopy-tetracorder).

Data availability. Data used in this paper are given in the main paper itself and in the Supplement. If needed, data are also available upon request by emailing the authors.

Author contribution. Sample permits were obtained by BLE, RG and AK. The samples were collected by CPG-P, AGR, AK, RG and XQ and analysed by AGR, MHC and NM. EMIT mineralogy maps we produced by RG, PB and RC. PG provided the FoO map. AGR analyzed the data and wrote of the original

draft manuscript supervised by CPG-P and XQ. CPG-P and XQ re-edited the manuscript and all authors contributed to data discussion, reviewing and manuscript finalization.

Competing interests. At least one of the (co-)authors is a member of the editorial board of Atmospheric chemistry and Physics.

Acknowledgements

We thank Richard Reynolds and another anonymous reviewer for the helpful comments and suggestions to improve the manuscript.

The field campaign and its associated research, including this work, was funded by the European Research Council under the Horizon 2020 research and innovation programme through the ERC Consolidator Grant FRAGMENT (grant agreement No. 773051) and the AXA Research Fund through the AXA Chair on Sand and Dust Storms at BSC. CGF was supported by a PhD fellowship from the Agència de Gestió d'Ajuts Universitaris i de Recerca (AGAUR) grant 2020_FI B 00678. KK was funded by the Deutsche Forschungsgemeinschaft (DFG, German Research Foundation) – 264907654; 416816480. MK has received funding through the Helmholtz Association's Initiative and Networking Fund (grant agreement no. VH-NG-1533). We acknowledge the EMIT project, which is supported by the NASA Earth Venture Instrument program, under the Earth Science Division of the Science Mission Directorate. We are grateful to Claire Blaske and Sahil Azad for assistance sampling in the Mojave National Preserve. Samples within the preserve were collected under permit MOJA-2022-SCI-0034. We thank Rose Pettiette at the BLM office in Needles, CA, for advice and allowing sampling on BLM land. We thank Jason Wallace and Anne Kelly from CSU Desert Studies Center at Zzyzx for their support during the campaign. BLE, RG, and AMK thank the Resnick Sustainability Institute at Caltech for partial support. Without all of them, the sampling campaign would not have been successfully feasible.

5. References

Alfaro, S. C., Gaudichet, A., Gomes, L., & Maillé, M. (1997). Modeling the size distribution of a soil aerosol produced by sandblasting. Journal of Geophysical Research: Atmospheres, 102(D10), 11239-11249.

Arnalds, Ó., Olafsson, H. and Dagsson-Waldhauserova, P.: Quantification of iron-rich volcanogenic dust emissions and deposition over the ocean from Icelandic dust sources, Biogeosciences, 11, 6623-6632. https://doi.org/10.5194/bg-11-6623-2014, 2014.

Atkinson, J. D., Murray, B. J., Woodhouse, M. T., Whale, T. F., Baustian, K. J., Carslaw, K. S., ... & Malkin, T. L.: The importance of feldspar for ice nucleation by mineral dust in mixed-phase clouds. Nature, 498(7454), 355-358, 2013.

Baddock, M. C., Ginoux, P., Bullard, J. E., & Gill, T. E. (2016). Do MODIS-defined dust sources have a geomorphological signature?. Geophysical Research Letters, 43(6), 2606-2613.

Baldo, C., Formenti, P., Nowak, S., Chevaillier, S., Cazaunau, M., Pangui, E., Di Baggio, C., Doussin, J.F., Ignatyev, K., Dagsson-Waldhauserova, P., Arnalds, O., MacKenzie, A.R., Shi, Z.: Distinct chemical and mineralogical composition of Icelandic dust compared to Northern African and Asian dust. Atmospheric Chemistry and Physics, 20, 13521-13539, 2020.

Bauer, S. E., & Koch, D.: Impact of heterogeneous sulfate formation at mineral dust surfaces on aerosol loads and radiative forcing in the Goddard Institute for Space Studies general circulation model. Journal of Geophysical Research: Atmospheres, 110(D17), 2005.

Beaudoing, H., Rodell, M., & NASA/GSFC/HSL: GLDAS Noah Land Surface Model L4 monthly 0.25 x 0.25 degree, Version 2.1 [dataset]. NASA Goddard Earth Sciences Data and Information Services Center. 2020. https://doi.org/10.5067/SXAVCZFAQLNO.

Buck, B.J., King, J. and Etyemezian, V., 2011. Effects of salt mineralogy on dust emissions, Salton Sea, California. Soil Science Society of America Journal, 75(5), pp.1971-1985.

Bullard, J. E., Harrison, S. P., Baddock, M. C., Drake, N., Gill, T. E., McTainsh, G., & Sun, Y. (2011). Preferential dust sources: A geomorphological classification designed for use in global dust-cycle models. Journal of Geophysical Research: Earth Surface, 116(F4).

Chatziparaschos, M., Daskalakis, N., Myriokefalitakis, S., Kalivitis, N., Nenes, A., Gonçalves Ageitos, M., Costa-Surós, M., Pérez García-Pando, C., Zanoli, M., Vrekoussis, M. & Kanakidou, M.: Role of K-feldspar and quartz in global ice nucleation by mineral dust in mixed-phase clouds. Atmospheric Chemistry and Physics, 23(3), 1785-1801, 2023.Cheary, R.W., Coelho, A.: A fundamental parameters approach to X-ray line profile fitting. Journal of Applied Crystallography 25, 109–121, 1992.

Claquin, T., Schulz, M., & Balkanski, Y. J. (1999). Modeling the mineralogy of atmospheric dust sources. Journal of Geophysical Research: Atmospheres, 104(D18), 22243-22256.

Clark, Roger N., 2024, PSI-edu/spectroscopy-tetracorder: Tetracorder 5.27 with expert systems to 5.27e + specpr, spectral libraries, and radiative transfer models (v5.27.0). Zenodo. https://doi.org/10.5281/zenodo.11204505

Clark, R. N., G. A. Swayze, K. E. Livo, P. Brodrick, E. Noe Dobrea, S. Vijayarangan, R. O. Green, D. Wettergreen, A. Candela, A. Hendrix, C. P. Garcia-Pando, N. Pearson, M. D. Lane, A. Gonzalez-Romero, X. Querol, and the EMIT and TREX teams, 2024. Imaging spectroscopy: Earth and planetary remote sensing with the PSI Tetracorder and expert systems: from Rovers to EMIT and Beyond Planetary Science Journal in review. Crumeyrolle, S., Gomes, L., Tulet, P., Matsuki, A., Schwarzenboeck, A., and Crahan, K.: Increase of the aerosol hygroscopicity by cloud processing in a mesoscale convective system: a case study from the AMMA campaign, Atmos. Chem. Phys., 8, 6907–6924, https://doi.org/10.5194/acp-8-6907-2008, 2008.

De la Torre, A.G., Bruque, S., Aranda, M.A.G.: Rietveld quantitative amorphous content analysis. Journal of Applied Crystallography, 34:196-202, 2001.

De Longueville, F., Hountondji Y.C., Henry S., Ozer P.: What do we know about effects of desert dust on air quality and human health in West Africa compared to other regions?. Sci. Total Environ., 409, 1–8, 2010.

Dibblee T.W.: Areal geology of the western mojave desert California. Geological Survey Professional paper, 522, https://doi.org/10.3133/pp522, 1967.

Di Biagio, C., Formenti, P., Balkanski, Y., Caponi, L., Cazaunau, M., Pangui, E., Journet, E., Nowak, S., Andreae, M.O., Kandler, K., Saeed, T., Piketh, S., Seibert, D., Williams, E., Doussin, J.F.: Complex refractive indices and single-scattering albedo of global dust aerosols in the shortwave spectrum and relationship to size and iron content. Atmos. Chem. Phys., 19, 15503-15531. https://doi.org/10.5194/acp-19-15503-2019, 2019.

Eghbal, M.K., Southard, R.J.: Mineralogy of Aridisols on Dissected Alluvial Fans, Western Mojave Desert, California. Soil Science Society of America Journal, 57, pp. 538-544, 1993.

Engelbrecht, J.P., Moosmüller, H., Pincock, S., Jayanty, R.K.M., Lersch, T., Casuccio, G.: Technical note: Mineralogical, chemical, morphological, and optical interrelationships of mineral dust re-suspensions. Atmos. Chem. Phys., 16, 10809-10830. https://doi.org/10.5194/acp-16-10809-2016, 2016.

Floyd, K. W., & Gill, T. E. (2011). The association of land cover with aeolian sediment production at Jornada Basin, New Mexico, USA. Aeolian Research, 3(1), 55-66.

Formenti, P., Caquineau, S., Chevaillier, S., Klaver, A., Desboeufs, K., Rajot, J.L., Belin, S., Briois, V.: Dominance of goethite over hematite in iron oxides of mineral dust from Western Africa: Quantitative partitioning by X-ray absorption spectroscopy. J. Geophys. Res. Atmos., 119, 12740-12754, https://doi.org/10.1002/2014jd021668, 2014.

Frank, T.D., Di Girolamo, L., Geegan, S.: The spatial and temporal variability of aerosol optical depths in the Mojave desert of southern California. Remote Sensing of Environment, 107, 1-2, 54-64, https://doi.org/10.1016/j.rse.2006.06.024, 2007.

Ginoux, P., Chin, M., Tegen, I., Prospero, J. M., Holben, B., Dubovik, O., & Lin, S. J. (2001). Sources and distributions of dust aerosols simulated with the GOCART model. Journal of Geophysical Research: Atmospheres, 106(D17), 20255-20273.

Ginoux, P., Prospero, J.M., Gill, T.E., Hsu, N.C., Zhao, M.: Global-scale attribution of anthropogenic and natural dust sources and their emission rates based on MODIS Deep Blue aerosol products. Rev. Geophys., 50, RG3005, doi:10.1029/2012RG000388, 2012.

Goldstein, H.L., Breit, G.N., & Reynolds, R.L.: Controls on the chemical composition of saline surface crusts and emitted dust from a wet playa in the Mojave Desert (USA). Journal of Arid Environments, 140, 50-66, 2017.

González-Flórez, C., Klose, M., Alastuey, A., Dupont, S., Escribano, J., Etyemezian, V., ... & Pérez García-Pando, C. (2022). Insights into the size-resolved dust emission from field measurements in the Moroccan Sahara. Atmospheric Chemistry and Physics Discussions, 2022, 1-65.

González-Romero, A., González-Florez, C., Panta, A., Yus-Díez, J., Reche, C., Córdoba, P., Moreno, N., Alastuey, A., Kandler, K., Klose, M., Baldo, C., Clark, R.N., Shi, Z.B., Querol, X., Pérez García-Pando, C.: Variability in grain size, mineralogy, and mode of occurence of Fe in surface sediments of preferential dust-source inland drainage basins: The case of the Lower Drâa Valley, S Morocco. Atmos. Chem. Phys., 23, 15815–15834, https://doi.org/10.5194/acp-23-15815-2023, 2023.

González-Romero, A., González-Florez, C., Panta, A., Yus-Díez, J., Córdoba, P., Alastuey, A., Moreno, N., Kandler, K., Klose, M., Clark, R.N., Ehlmann, B.L., Greenberger, R., Keebler, A.M., Brodick, P., Green, R., Querol, X., Pérez García-Pando, C.: Probing Iceland's Dust-Emitting Sediments: Particle Size Distribution, Mineralogy, Cohesion, Fe Mode of Occurrence, and Reflectance Spectra Signatures. Atmospheric Chemistry and Physics. EGUSPHERE [Preprint], 2024.

Goudie, A.: Dust storms and ephemeral lakes. Desert, 23(1), 153-164, 2018.

Goudie, A.S. & Middleton, N.J.: Desert dust in the global system. Springer, Heidelberg. ISBN 978-786 3-540-32355-6, 288 pp, 2006.

Green R.O., Mahowald N., Ung C., Thompson D.R., Bator L., Bennet M., Zan J.: The earth surface mineral dust source investigation: an earth science imaging spectroscopy mission. In: IEEE Aerospace Conference Proceedings. IEEE Computer Society. https://doi.org/10.1109/AERO47225.2020.9172731. 2020.

Harrison, A. D., Lever, K., Sanchez-Marroquin, A., Holden, M. A., Whale, T. F., Tarn, M. D., ... & Murray, B. J.: The ice-nucleating ability of quartz immersed in water and its atmospheric importance compared to K-feldspar. Atmospheric Chemistry and Physics, 19(17), 11343-11361, 2019.

Hettiarachchi, E., Reynolds, R. L., Goldstein, H. L., Moskowitz, B., & Rubasinghege, G. Bioavailable iron production in airborne mineral dust: Controls by chemical composition and solar flux. Atmospheric environment, 205, 90-102, 2019.

Hettiarachchi, E., Ivanov, S., Kieft, T., Goldstein, H. L., Moskowitz, B. M., Reynolds, R. L., & Rubasinghege, G. Atmospheric processing of iron-bearing mineral dust aerosol and its effect on growth of a marine diatom, Cyclotella meneghiniana. Environmental Science & Technology, 55(2), 871-881, 2020.

Honke, J.S., Pigati, J.S., Wilson, J., Bright, J., Goldstein, H.L., Skipp, G.L., Reheis, M.C., Havens, J.C.: Late Quaternary paleohydrology of desert wetlands and pluvial lakes in the Soda Lake basin, central Mojave Desert, California (USA). Quat. Sci. Rev., 216, pp. 89-106, 10.1016/j.quascirev.2019.05.021, 2019.

Ibáñez, J., Font, O., Moreno, N., Elvira, J.J., Alvarez, S., Querol, X.: Quantitative Rietveld analysis of the crystalline and amorphous phases in coal fly ashes. Fuel, 105: 314-317, 2013.

Jennings, C.W., Burnett, J.L., and Troxel, B.W.: Geologic map of California: Trona sheet. California Division of Mines and Geology, Geologic Atlas of California, GAM-23, 1:250.000, 1962.

Jickells, T. D., An, Z. S., Andersen, K. K., Baker, A. R., Bergametti, G., Brooks, N., ... & Torres, R.: Global iron connections between desert dust, ocean biogeochemistry, and climate. science, 308(5718), 67-71, 2005.

Journet, E., Balkanski, Y., & Harrison, S. P. (2014). A new data set of soil mineralogy for dust-cycle modeling. Atmospheric Chemistry and Physics, 14(8), 3801-3816.

Karanasiou, A., Moreno, N., Moreno, T., Viana, M., de Leeuw, F., Querol, X.: Health effects from Sahara dust episodes in Europe: Literature review and research gaps. Environ. Int. 47, 107–14, 2012.

Kok, J.F., Adebiyi, A.A., Albani, S., Balkanski, Y., Checa-Garcia, R., Chin, M., Colarco, P.R., Hamilton, D.S., Huang, Y., Ito, A., Klose, M., Li, L., Mahowald, N.M., Miller, R.L., Obiso, V., Pérez García-Pando, C., Rocha-Lima, A., Wan, J.S.: Contribution of the world's main dust source regions to the global cycle of desert dust, Atmos. Chem. Phys., 21, 8169–8193, https://doi.org/10.5194/acp-21-8169-2021, 2021.

Laurent, B., Marticorena, B., Bergametti, G., Léon, J.F., Mahowald, N.M.: Modeling Mineral Dust Emissions from the Sahara Desert Using New Surface Properties and Soil Database J. Geophys. Res., 113, D14218, 2008.

Li, L., Mahowald, N. M., Miller, R. L., Pérez García-Pando, C., Klose, M., Hamilton, D. S., ... & Thompson, D. R. (2021). Quantifying the range of the dust direct radiative effect due to source mineralogy uncertainty. Atmospheric chemistry and physics, 21(5), 3973-4005.

Machiels, L., Mertens, G., Elsen, J.: Rietveld Refinement strategy for Quantitative Phase analysis of Partially Amorphous zeolitized tuffaceous. GEOLOGICA BELGICA 13,3, 183-196, 2010.

Madsen, I.C., Scarlett, N.V.Y., Cranswick, L.M.D., Lwin, T.: Outcomes of the international union of crystallography commission on powder diffraction round robin on quantitative phase analysis: Samples 1a to 1h. J. Appl. Crystallogr., 34, pp. 409-426, 2001.

Mahowald, N.M., Baker, A.R., Bergametti, G., Brooks, N., Duce, R.A., Jickells, T.D., Kubilay, N., Prospero, J.M., Tegen, I.: Atmospheric global dust cycle and iron inputs to the ocean, Global Biogeochem. Cy., 19(4), GB4025, doi:10.1029/2004GB002402, 2005.

Matsui, H., Yamane, M., Tonami, T., Nagami, T., Watanabe, K., Kishi, R., Kitagawa, Y., Nakano, M.: Theoretical study on gigantic effect of external static electric field application on nonlinear optical properties of 1,2,3,5-dithiadiazolyl π-radical dimer. Mater. Chem. Front., 2, 785– 790, DOI: 10.1039/C7QM00549K, 2018.

Miller, D.M., Menges, C.M., and Lidke, D.J.: Generalized surficial geologic map of the Fort Irwin area, San Bernardino County, California, U.S. Geological Survey, Open-File Report OF-2013-1024-B, 1:100.000, 2014.

Miller, D.M., Dudash, S.L., & McGeehin, J.P.: Paleoclimate record for Lake Coyote, California, and the Last Glacial Maximum and deglacial paleohydrology (25 to 14 cal ka) of the Mojave River. S.W. Starratt, M.R. Rosen (Eds.), From Saline to Freshwater: The Diversity of Western Lakes in Space and Time: Geologic Society of America Special Paper 536, pp. 1-20, 2018.

Nield, J.M., Bryant, R.G., Wiggs, G.F., King, J., Thomas, D.S., Eckardt, F.D., and Washington, R. The dynamism of salt crust patterns on playas. Geology, 43(1), pp.31-34, 2015.

Nield, J.M., Neuman, C.M., O'Brien, P., Bryant, R.G., and Wiggs, G.F. Evaporative sodium salt crust development and its wind tunnel derived transport dynamics under variable climatic conditions. Aeolian Research, 23, pp.51-62, 2016.

Nield, J.M., Wiggs, G.F., King, J., Bryant, R.G., Eckardt, F.D., Thomas, D.S. and Washington, R. Climate–surface–pore-water interactions on a salt crusted playa: implications for crust pattern and surface roughness development measured using terrestrial laser scanning. Earth Surface Processes and Landforms, 41(6), pp.738-753, 2016.

Obiso, V., Gonçalves Ageitos, M., Pérez García-Pando, C., Perlwitz, J. P., Schuster, G. L., Bauer, S. E., ... & Miller, R. L. (2024). Observationally constrained regional variations of shortwave absorption by iron oxides emphasize the cooling effect of dust. Atmospheric Chemistry and Physics, 24(9), 5337-5367.

Panta, A., Kandler, K., Alastuey, A., González-Flórez, C., González-Romero, A., Klose, M., ... & Pérez García-Pando, C. (2022). Insights into the single particle composition, size, mixing state and aspect ratio of freshly emitted mineral dust from field measurements in the Moroccan Sahara using electron microscopy. Atmospheric Chemistry and Physics Discussions, 2022, 1-40.

Paulot, F., Ginoux, P., Cooke, W. F., Donner, L. J., Fan, S., Lin, M. Y., ... & Horowitz, L. W. (2016). Sensitivity of nitrate aerosols to ammonia emissions and to nitrate chemistry: implications for present and future nitrate optical depth. Atmospheric Chemistry and Physics, 16(3), 1459-1477.

Pérez, C., Nickovic, S., Pejanovic, G., Baldasano, J. M., & Özsoy, E.: Interactive dust-radiation modeling: A step to improve weather forecasts. Journal of Geophysical Research: Atmospheres, 111(D16), 2006.

Pérez García-Pando, C., Stanton, M.C., Diggle, P.J., Trzaska, S., Miller, R.L., Perlwitz, J.P., Baldasano, J.M., Cuevas, E., Ceccato, P., Yaka, P., Thomson, M.C.: Soil dust aerosols and wind as predictors of seasonal meningitis incidence in Niger. Environ. Health Perspect. 122, 7679-686, 2014.

Perlwitz, J.P., Pérez García-Pando, C., and Miller, R.L.: Predicting the mineral composition of dust aerosols – Part 1: Representing key processes. Atmos. Chem. Phys., 15, 11593–11627, https://doi.org/10.5194/acp-15-11593-2015, 2015.

Potter, C. and Coppernoll-Houston, D.: Controls on land surface temperature in deserts of southern california derived from MODIS satellite time series analysis, 2000 to 2018. Climate, 7, 32, https://doi.org/10.3390/cli7020032, 2019.

Querol, X.: The Occurrence and Distribution of Trace Elements in the Teruel Mining District Coals and their Behaviour during Coal Combustion. European Coal and Steel Community Project 7220/ED/014, 1993.

Querol, X., Whateley, M.K.G., Fernandez-Turiel, J.L., Tuncali, E.: Geological controls on the mineralogy and geochemistry of the Beypazari lignite, Central Anatolia, Turkey. Int. J. Coal. Geol., 33:255–271, 1997.

Raupach, M.R., Gillette, D.A., Leys, J.F.: The effect of roughness elements on wind erosion threshold. J. Geophys. Res., 98, 3023-3029, 1993.

Reheis, M.C., Goodmacher, J.C., Harden, J.W., McFadden, L.D., Rockwell, T.K., Shroba, R.R., Sowers, J.M. and Taylor, E.M. Quaternary soils and dust deposition in southern Nevada and California. Geological Society of America Bulletin, 107(9), pp.1003-1022, 1995.

Reheis, M.C. and Kihl, R. Dust deposition in southern Nevada and California, 1984–1989: Relations to climate, source area, and source lithology. Journal of Geophysical Research: Atmospheres, 100(D5), pp.8893-8918, 1995.

Reheis, M.C. Dust deposition downwind of Owens (dry) Lake, 1991–1994: Preliminary findings. Journal of Geophysical Research: Atmospheres, 102(D22), pp.25999-26008, 1997.

Reheis, M.C., Budahn, J.R. and Lamothe, P.J. Geochemical evidence for diversity of dust sources in the southwestern United States. Geochimica et Cosmochimica Acta, 66(9), pp.1569-1587, 2002.

Reheis, M.C., Budahn, J.R., Lamothe, P.J. and Reynolds, R.L. Compositions of modern dust and surface sediments in the Desert Southwest, United States. Journal of Geophysical Research: Earth Surface, 114(F1), 2009.

Reheis, M.C., Bright, J., Lund, S.P., Miller, D.M., Skipp, G., Fleck, R.J.: A half-million-year record of paleoclimate from the Lake Manix core, Mojave Desert, California. Palaeogeogr., Palaeoclim. Palaeoecol., 365–366, pp. 11-37, 2012.

Reynolds, R.L., Reheis, M., Yount, J. and Lamothe, P. Composition of aeolian dust in natural traps on isolated surfaces of the central Mojave Desert—Insights to mixing, sources, and nutrient inputs. Journal of Arid Environments, 66(1), pp.42-61, 2006.

Reynolds, R.L., Yount, J.C., Reheis, M., Goldstein, H., Chavez Jr, P., Fulton, R., Whitney, J., Fuller, C. and Forester, R.M. Dust emission from wet and dry playas in the Mojave Desert, USA. Earth Surface Processes and Landforms: The Journal of the British Geomorphological Research Group, 32(12), pp.1811-1827, 2007.

Reynolds, R.L., Bogle, R., Vogel, J., Goldstein, H., Yount, J.: Dust emission at Franklin Lake Playa, Mojave Desert (USA): Response to meteorological and hydrologic changes 2005–2008, in: Oren, A., Naftz, D. L., Wurtsbaugh, W. A. (Eds.), Saline lakes around the world: unique systems with unique values, Natural Resources and Environmental Issues 15, 105–116, https://digitalcommons.usu.edu/nrei/vol15/iss1/18 (last access: 7 November 2023), 2009.

Rietveld, H.M.: A profile refinement method for nuclear and magnetic structures. Journal of Applied Crystallography 2, 65–71, 1969.

Scanza, R. A., Mahowald, N., Ghan, S., Zender, C. S., Kok, J. F., Liu, X., ... & Albani, S. (2015). Modeling dust as component minerals in the Community Atmosphere Model: development of framework and impact on radiative forcing. Atmospheric Chemistry and Physics, 15(1), 537-561.

Scarlett, N. & Madsen, I.: Quantification of phases with partial or no known crystal structures. Powder Diffraction, 21(4), 278-284, 2006.

Shao, Y., Raupach, M.R., & Findlater, P.A.: Effect of saltation bombardment on the entrainment of dust by wind. Journal of Geophysical Research: Atmospheres, 98(D7), 12719-12726, 1993.

Shao, Y. (2001). A model for mineral dust emission. Journal of Geophysical Research: Atmospheres, 106(D17), 20239-20254.

Shao, Y., Wyrwoll, K. H., Chappell, A., Huang, J., Lin, Z., McTainsh, G. H., ... & Yoon, S. (2011). Dust cycle: An emerging core theme in Earth system science. Aeolian Research, 2(4), 181-204.

Shi, Z.B., Krom, M.D., Bonneville, S.: Formation of Iron Nanoparticles and Increase in Iron Reactivity in Mineral Dust during Simulated Cloud Processing. Environ. Sci. Technol. 43, 6592-6596, 2009.

Sperazza, M., Moore, J.N., Hendrix, M.: High-Resolution particle size analysis of naturally occurring very fine-grained sediment through laser diffractometry. J. Sediment. Res., 74 (5), 736-743, 2004.

Stout, J. E., & Lee, J. A. (2003). Indirect evidence of wind erosion trends on the Southern High Plains of North America. Journal of Arid Environments, 55(1), 43-61.

Sullivan, R.C., Guazzotti, S.A., Sodeman, D.A., Tang, Y., Carmichael, G.R., & Prather, K.A.: Mineral dust is a sink for chlorine in the marine boundary layer. Atmospheric Environment, 41(34), 7166–7179, 2007.

Thorez, J.: Practical Identification of Clay Minerals: A Handbook for Teachers and Students in Clay Mineralogy. Institute of mineralogy, Liège State University, Belgium, Lelotte Eds, B 4820 DISON (Belgique),90pg, 1976.

Tong, D.Q., Dan, M., Wang, T., Lee, P.: Long-term dust climatology in the western United States reconstructed from routine aerosol ground monitoring, Atmos. Chem. Phys., 12, 5189–5205, https://doi.org/10.5194/acp-12-5189-2012, 2012.

TOPAS: TOPAS and TOPAS-Academic: an optimization program integrating computer algebra and crystallographic objects written in C++. J. Appl. Cryst. (2018). 51, 210-218, 2018.

Urban, F.E., Reynolds, R.L., Fulton, R.: The dynamic interaction of climate, vegetation, and dust emission, Mojave Desert, USA. A. Fernandez-Bernal, M.A. De La Rosa (Eds.), Arid Environments and Wind Erosion, NOVA Science Publishers, Inc., pp. 243-267, 2009.

Urban, F.E., Goldstein, H.L., Fulton, R., Reynolds, R.L.: Unseen dust emission and global dust abundance: documenting dust emission from the Mojave Desert (USA) by daily remote camera imagery and wind-erosion measurements. J. Geophys. Res. Atmos., 123 (16), pp. 8735-8753, 2018.

USGS, U. S. Geological Survey Open-File Report 01-041. A Laboratory Manual for X-Ray Powder Diffraction https://pubs.usgs.gov/of/2001/of01-041/htmldocs/methods/oamount.htm. Last access: 17th January of 2024.

Vandenberghe, R. E., Barrero, C. A., Da Costa, G. M., Van San, E., and De Grave, E.: Mössbauer characterization of iron oxides and (oxy) hydroxides: the present state of the art. Hyperfine Interactions, 126, 247-259, 2000.

Weaver, C., Ginoux, P., Hsu, N., Chou, M.-D., Joiner, J.: Radiative forcing of Saharan dust: GOCART model simulations compared with ERBE data. J. Atmos. Sci., 59, 736-747, 2002.

Whitney, J.W., Breit, G.N., Buckingham, S.E., Reynolds, R.L., Bogle, R.C., Luo, L., Goldstein, H.L., Vogel, J.M.: Aeolian responses to climate variability during the past century on Mesquite Lake Playa, Mojave Desert. Geomorphology, 230, 13-25, 2015.

Young, R.A.: The Rietveld method. International Union of Crystallography. Oxford University Press, UK, 1993.

Zubko, N., Munoz, O., Zubko, E., Gritsevich, M., Escobar-Cerezo, J., Berg, M. J. and Peltoniemi, J.: Light scattering from volcanic-sand particles in deposited and aerosol form. Atmospheric Environment, 215, 116813. https://doi.org/10.1016/j.atmosenv.2019.06.051, 2019.

Figure captions:

Figure 1: Study area map including the playa lakes studied together with a geologic map, simplified from Jennings et al. (1962) and Miller et al. (2014). The star represents the Zzyzx complex and green dots the samples used in this study. Basemap: Imagery data from © Google Earth Pro v: 7.3.6.9345.

Figure 2: Map of Frequency of Occurrence (FoO) of dust optical depth > 0.1 over the study region derived from MODIS C6.1 Aqua (1:30PM equatorial passing time) Level 2 Deep Blue aerosol products at 0.1 degree resolution. A dust occurrence is counted when DOD > 0.1, Angstrom Exponent < 0.3 and DOD at 412 nm > DOD at 470 nm. Blue iso-contours represent 5 and 10 % of daily occurrences per year averaged over 20 years (2003-2022). Green dots represent the samples collected and used in this study. Basemap: Imagery data from © Google Earth Pro v: 7.3.6.9345.

Figure 3: EMIT scenes emit20231015T215209_color-visRGB and emit20230728T214142_color-visRGB at 60 m per pixel showing the diversity of Fe^{2+}, Fe^{3+} and Fe^{2+} and Fe^{3+} bearing minerals and the carbonates, salt and phyllosilicates minerals.

Figure 4: Examples of samples collected in the Mojave Desert including crusts (a), aeolian ripples (b), massive compact crust (c) and a salty spongy crust (d).

Figure 5: Fully dispersed particle size distribution (FDPSD) and minimally dispersed particle size distribution (MDPSD) for crusts and aeolian ripples from the Mojave Desert (median PSD from all the samples), Soda, Mesquite, Cronese, Ivanpah and Coyote Lakes. In shaded blue and brown the standard deviation of each PSD (nº of samples used in Table 1), except for Ivanpah and Coyote Lakes (only 1 sample each).

Figure 6: % of mass fractions from the dry sieved size fractions (250-50, 80-250, 63-80, 40-63, 20-40 and <20 µm). The range of the enrichment factors of each mineral group for each dry size fraction of the 16 crust samples (blue) and for the 4 aeolian ripples samples (red).

Figure 7: Box-plot showing averaged mineral contents for all samples, crusts and aeolian ripples (wt %).

Figure 8: Geological cross section and mineralogy of the crusts of the Soda Lake. Top panel represent major mineralogy composition. Mid panel represents the position of the samples, the Zzyzx complex, and the path of the cross section. Bottom schematic cross section simplifying the position in the basin. Basemap: Imagery data from © Google Earth Pro v: 7.3.6.9345.

Figure 9: Cross-correlation plots of the clay contents and amphibole with the FeT (a) and clay minerals and FeA (b), all in wt % in crusts.

Figure 10: Modes of occurrence of Fe comparison between the crusts (C) playa lakes analysed in this study, the average of the crusts and ripples (R) at Mojave Desert, Morocco and Iceland Top surface (TS). FeA is referred to the exchangeable Fe and nano Fe oxides, FeD is the Fe content in hematite and goethite, FeM is the Fe content in maghemite/magnetite and FeS is the Fe content in Fe bearing minerals.

Figure 11: Conceptual model of wet and dry playa lakes differences due to groundwater differences and how this can affect the mineralogy of the surface in the playa lakes. Also illustrated is the expected dust emission rate, major mineralogy and modes of occurrence of Fe differences expected in the emitted dust.

Figure 1.

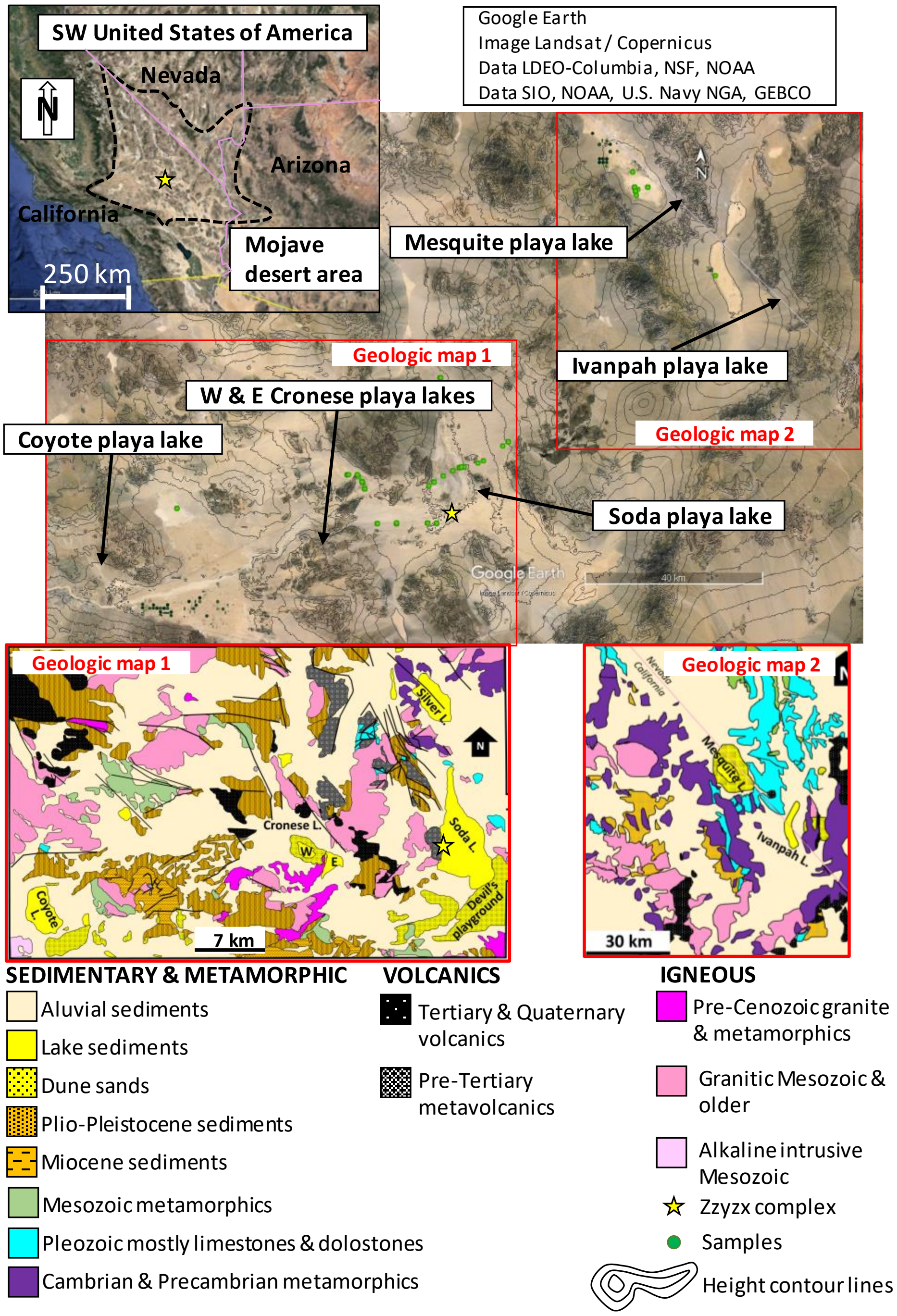
SW United States of America
N
Nevada
Arizona
California
250 km
Mojave desert area
Google Earth
Image Landsat / Copernicus
Data LDEO-Columbia, NSF, NOAA
Data SIO, NOAA, U.S. Navy NGA, GEBCO
Mesquite playa lake
Ivanpah playa lake
Geologic map 2
Geologic map 1
W & E Cronese playa lakes
Coyote playa lake
Soda playa lake
Google Earth
40 km
Geologic map 1
Silver L.
Cronese L.
W
E
Soda L.
Devil's playground
Coyote L.
7 km
Geologic map 2
Nevada
California
Mesquite L.
Ivanpah L.
30 km
SEDIMENTARY & METAMORPHIC
Aluvial sediments
Lake sediments
Dune sands
Plio-Pleistocene sediments
Miocene sediments
Mesozoic metamorphics
Pleozoic mostly limestones & dolostones
Cambrian & Precambrian metamorphics
VOLCANICS
Tertiary & Quaternary volcanics
Pre-Tertiary metavolcanics
IGNEOUS
Pre-Cenozoic granite & metamorphics
Granitic Mesozoic & older
Alkaline intrusive Mesozoic
Zzyzx complex
Samples
Height contour lines

Figure 2.

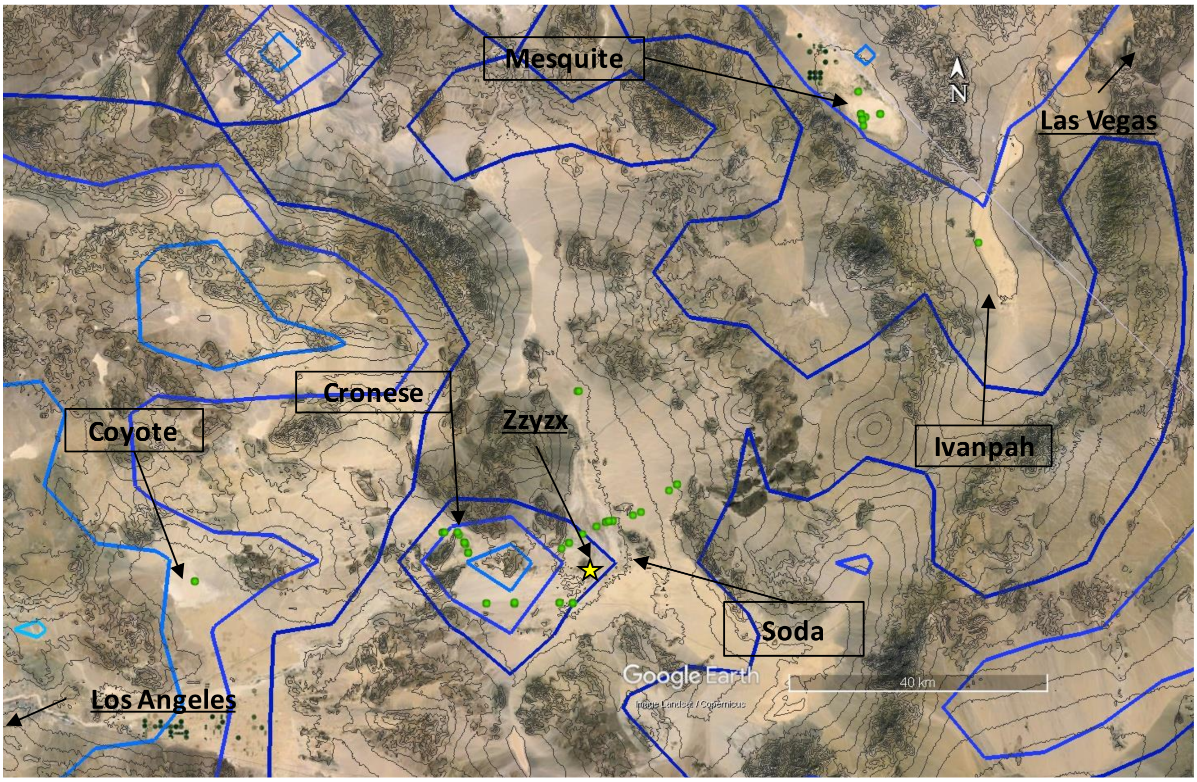
Mesquite
N
Las Vegas
Cronese
Coyote
Zzyzx
Ivanpah
Soda
Google Earth
40 km
Image Landsat / Copernicus
Los Angeles

Figure 3.

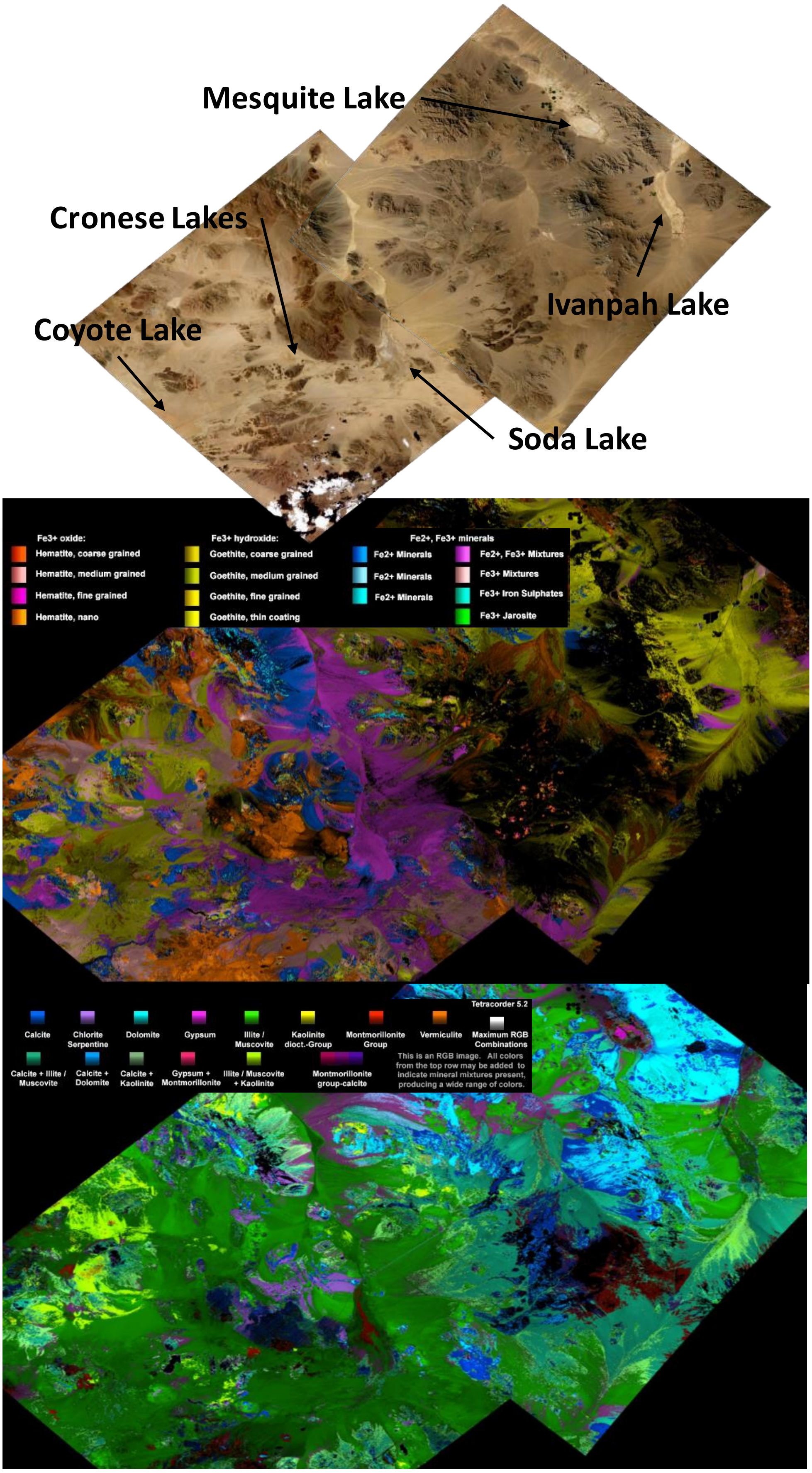
Mesquite Lake
Cronese Lakes
Ivanpah Lake
Coyote Lake
Soda Lake
Fe3+ oxide:
Hematite, coarse grained
Hematite, medium grained
Hematite, fine grained
Hematite, nano
Fe3+ hydroxide:
Goethite, coarse grained
Goethite, medium grained
Goethite, fine grained
Goethite, thin coating
Fe2+, Fe3+ minerals
Fe2+ Minerals
Fe2+ Minerals
Fe2+ Minerals
Fe2+, Fe3+ Mixtures
Fe3+ Mixtures
Fe3+ Iron Sulphates
Fe3+ Jarosite
Tetracorder 5.2
Calcite
Chlorite Serpentine
Dolomite
Gypsum
Illite / Muscovite
Kaolinite dioct.-Group
Montmorillonite Group
Vermiculite
Maximum RGB Combinations
Calcite + Illite / Muscovite
Calcite + Dolomite
Calcite + Kaolinite
Gypsum + Montmorillonite
Illite / Muscovite + Kaolinite
Montmorillonite group-calcite
This is an RGB image. All colors from the top row may be added to indicate mineral mixtures present, producing a wide range of colors.

Figure 4.

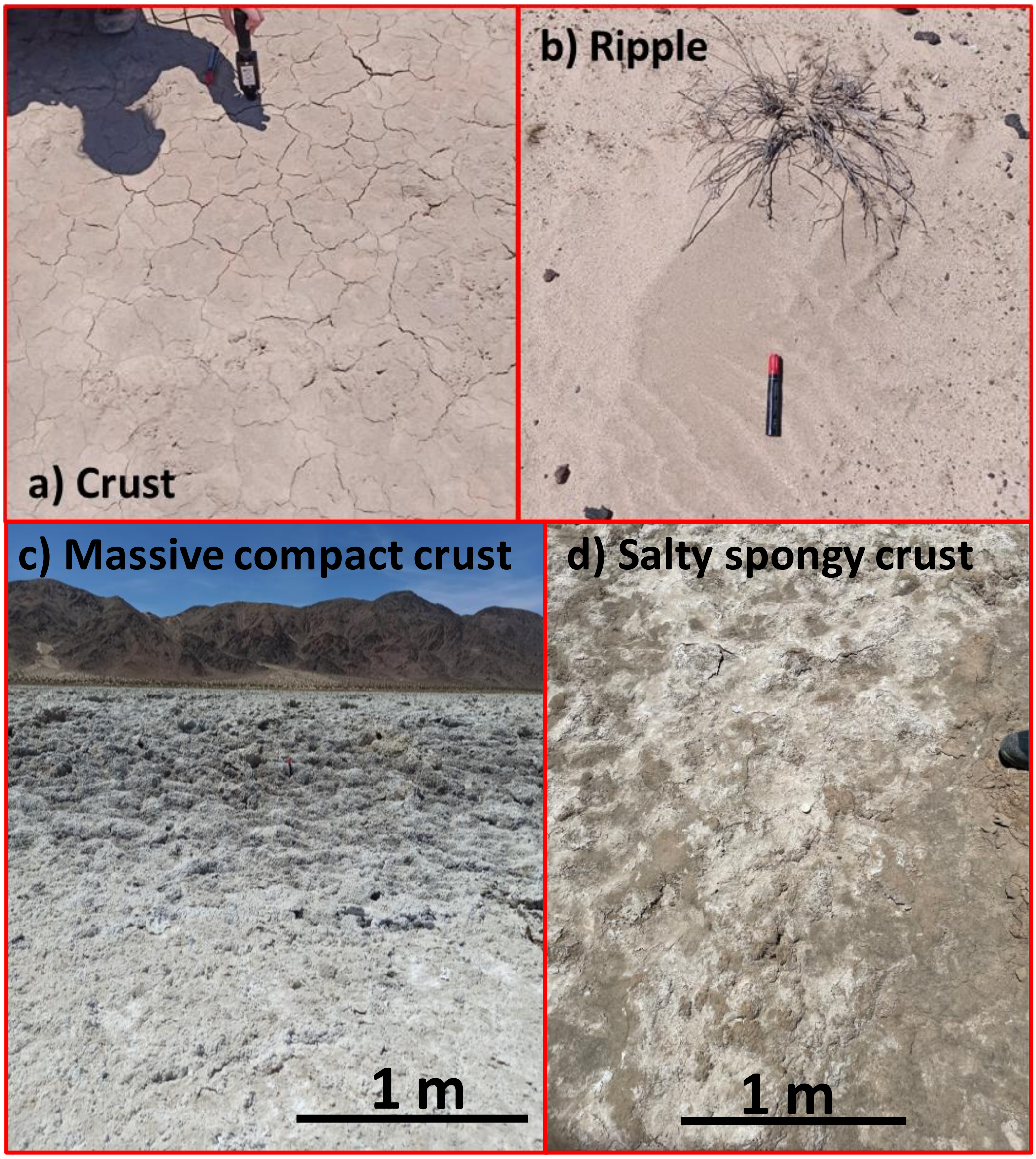
a) Crust
b) Ripple
c) Massive compact crust
d) Salty spongy crust
1 m
1 m

Figure 5.

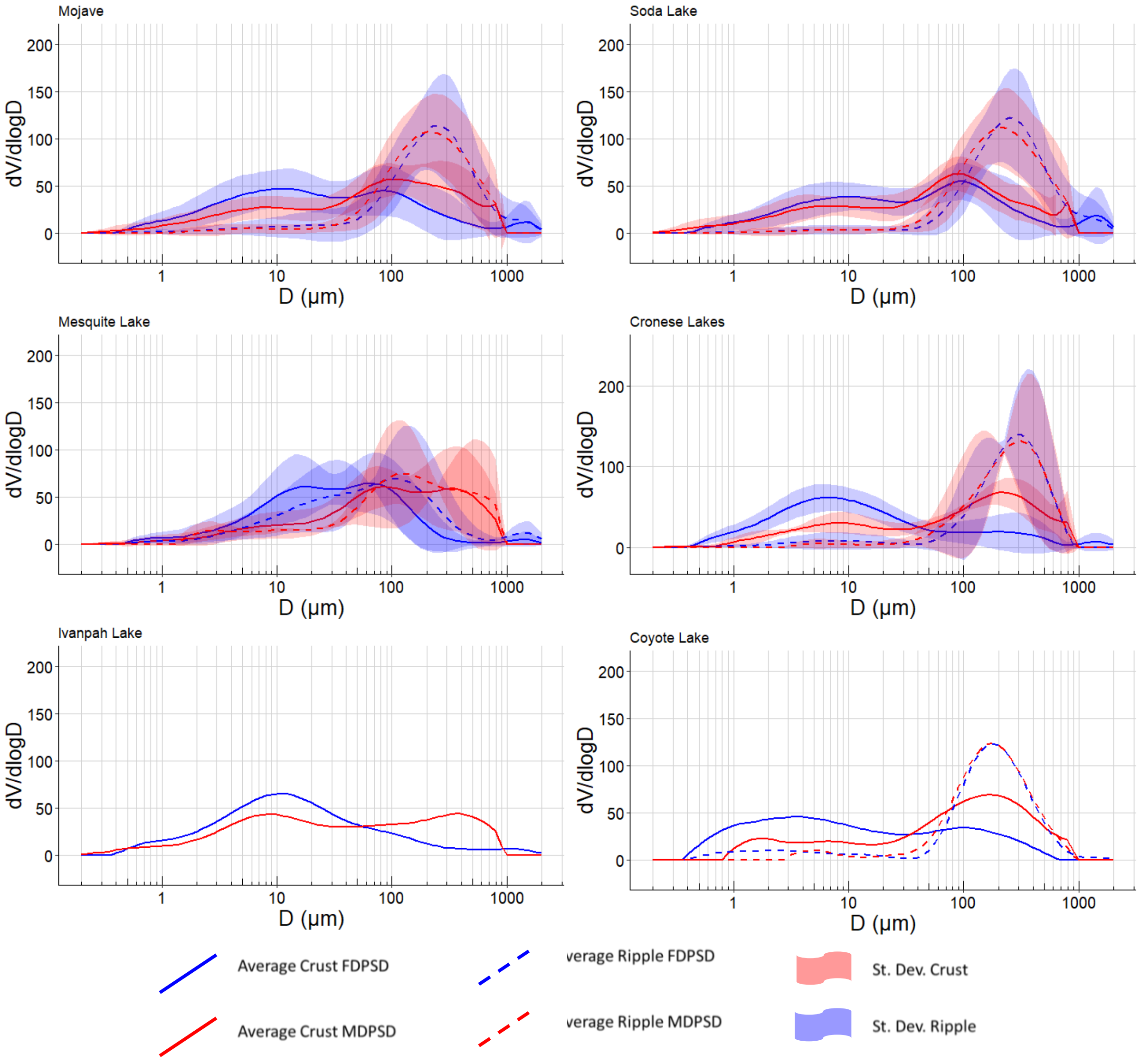
Mojave
Soda Lake
Mesquite Lake
Cronese Lakes
Ivanpah Lake
Coyote Lake
dV/dlogD
0
50
100
150
200
1
10
100
1000
D (µm)
Average Crust FDPSD
Average Crust MDPSD
verage Ripple FDPSD
verage Ripple MDPSD
St. Dev. Crust
St. Dev. Ripple

1057 Figure 6.

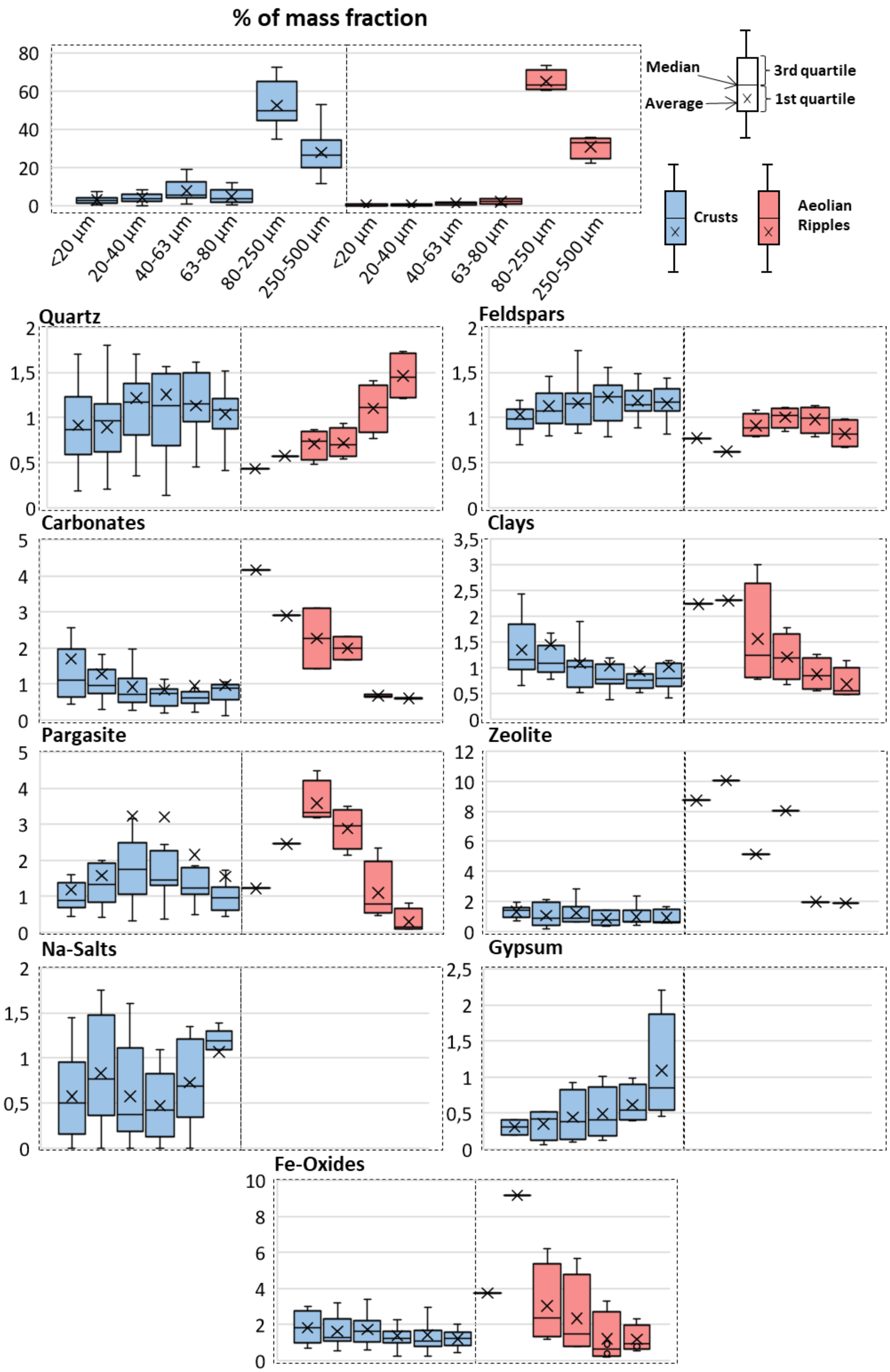

1058

Figure 7.

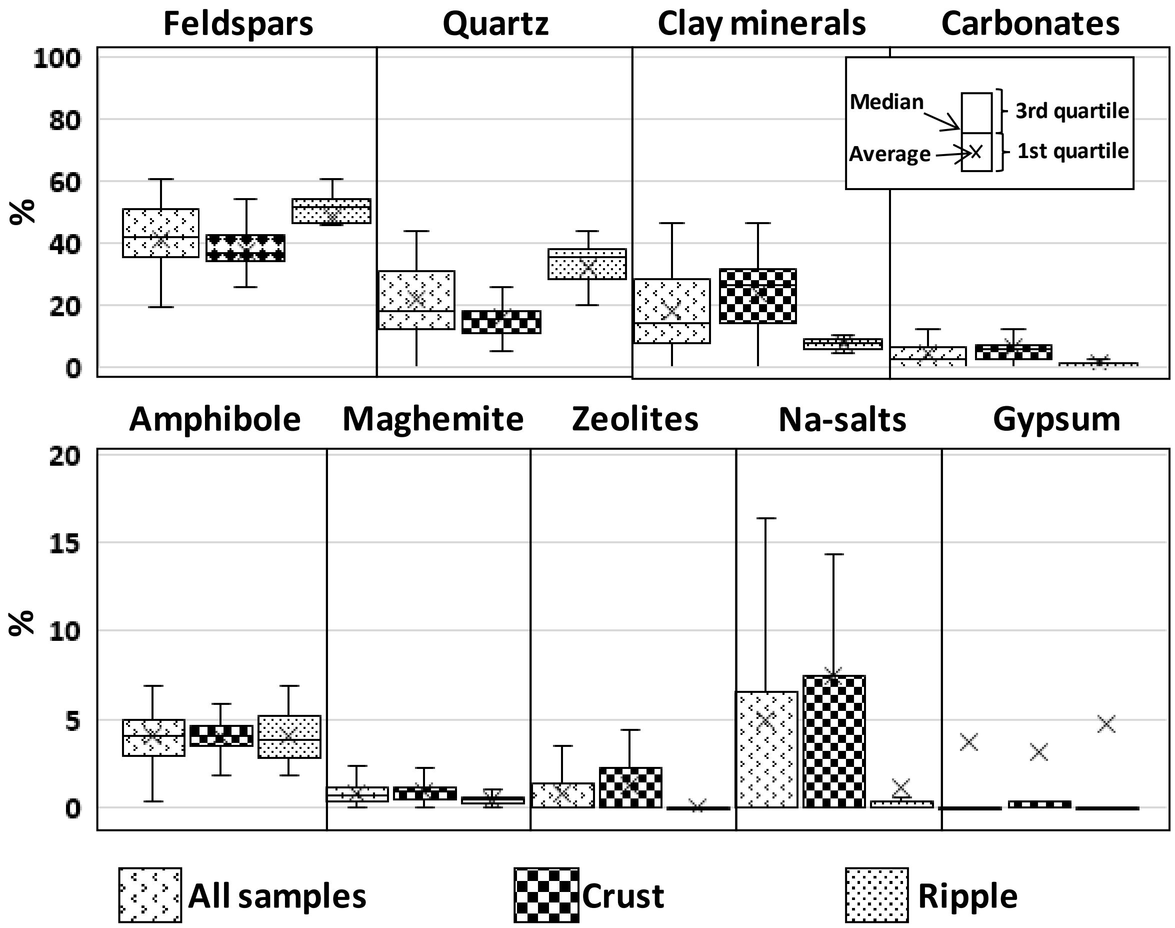
Feldspars
Quartz
Clay minerals
Carbonates
100
80
60
40
20
0
%
Median
Average
3rd quartile
1st quartile
Amphibole
Maghemite
Zeolites
Na-salts
Gypsum
20
15
10
5
0
%
All samples
Crust
Ripple

Figure 8.

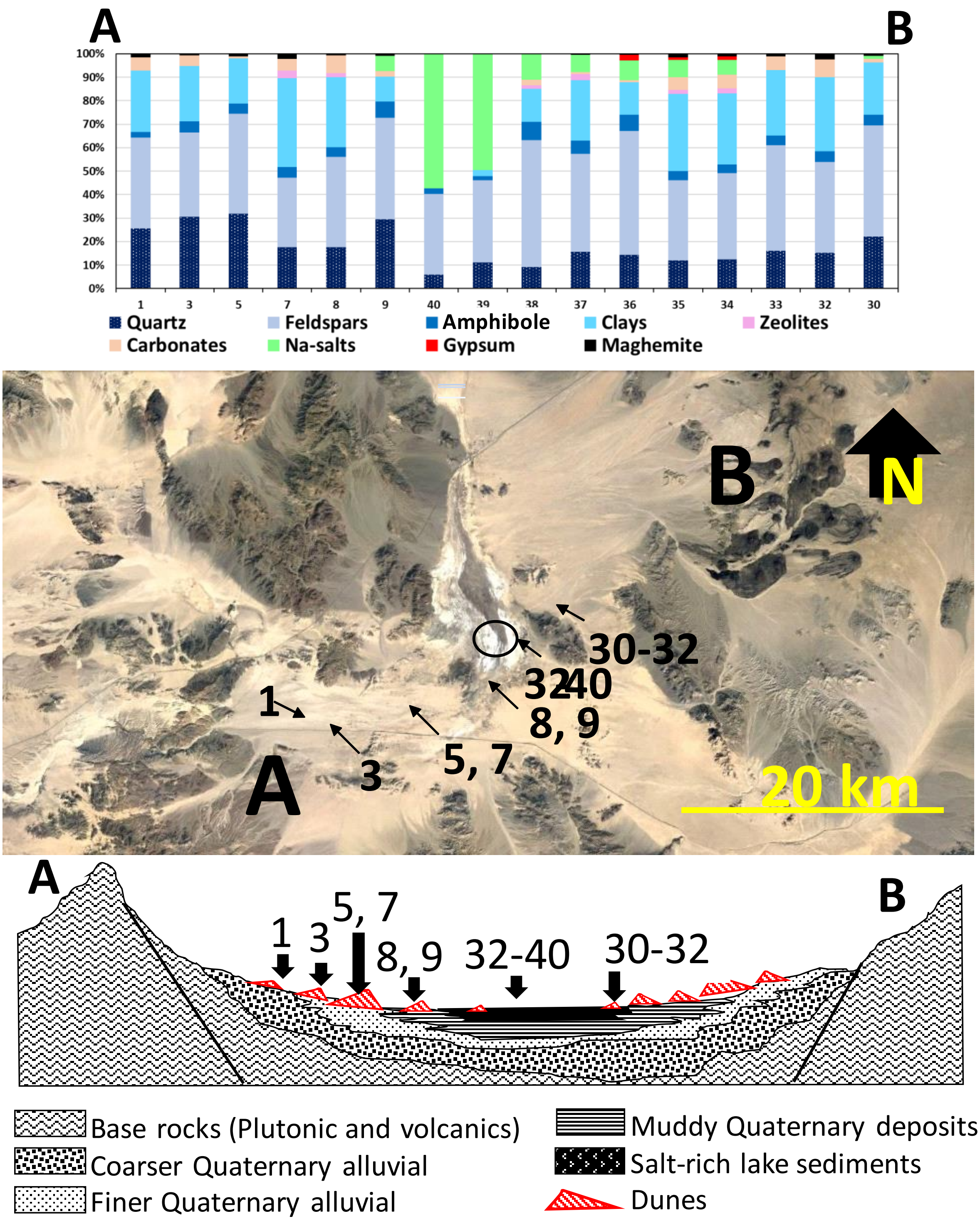
A
B
100%
90%
80%
70%
60%
50%
40%
30%
20%
10%
0%
1
3
5
7
8
9
40
39
38
37
36
35
34
33
32
30
Quartz
Feldspars
Amphibole
Clays
Zeolites
Carbonates
Na-salts
Gypsum
Maghemite
B
N
30-32
32-40
8, 9
1
3
5, 7
A
20 km
A
B
5, 7
1
3
8, 9
32-40
30-32
Base rocks (Plutonic and volcanics)
Coarser Quaternary alluvial
Finer Quaternary alluvial
Muddy Quaternary deposits
Salt-rich lake sediments
Dunes

Figure 9.

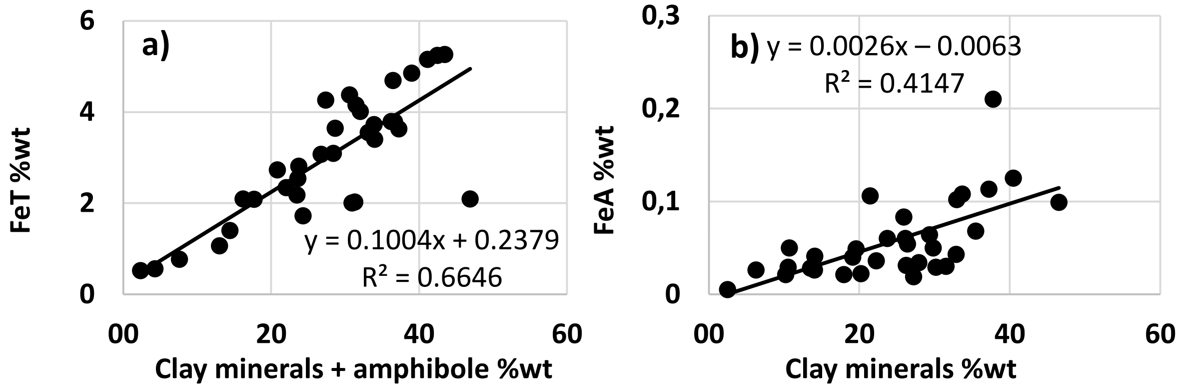
a)
FeT %wt
6
4
2
0
00
20
40
60
Clay minerals + amphibole %wt
y = 0.1004x + 0.2379
R^2 = 0.6646
b) y = 0.0026x – 0.0063
R^2 = 0.4147
FeA %wt
0,3
0,2
0,1
0
00
20
40
60
Clay minerals %wt

Figure 10.

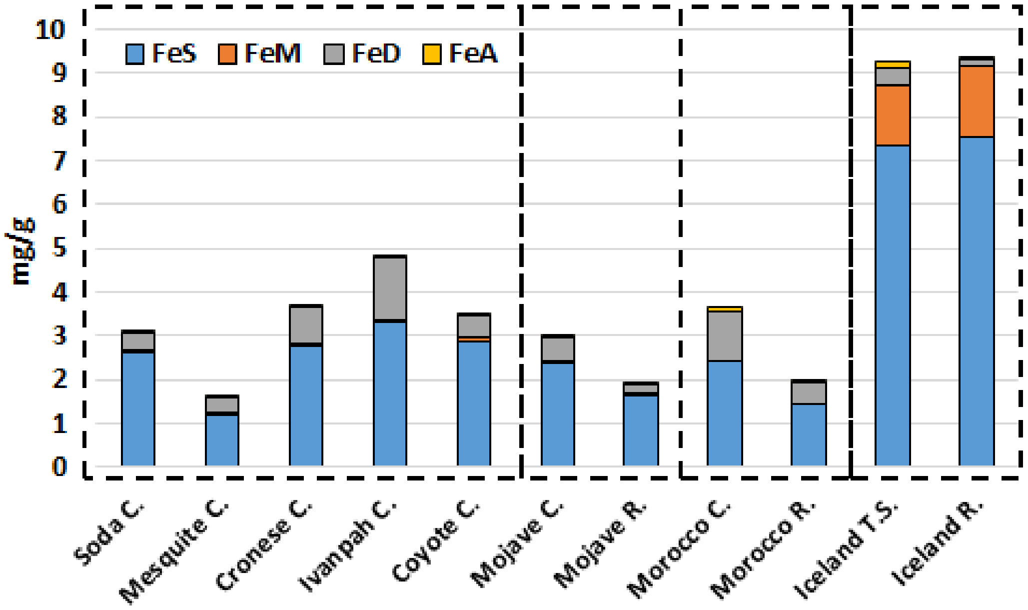
FeS
FeM
FeD
FeA
mg/g
0
1
2
3
4
5
6
7
8
9
10
Soda C.
Mesquite C.
Cronese C.
Ivanpah C.
Coyote C.
Mojave C.
Mojave R.
Morocco C.
Morocco R.
Iceland T.S.
Iceland R.

Figure 11.

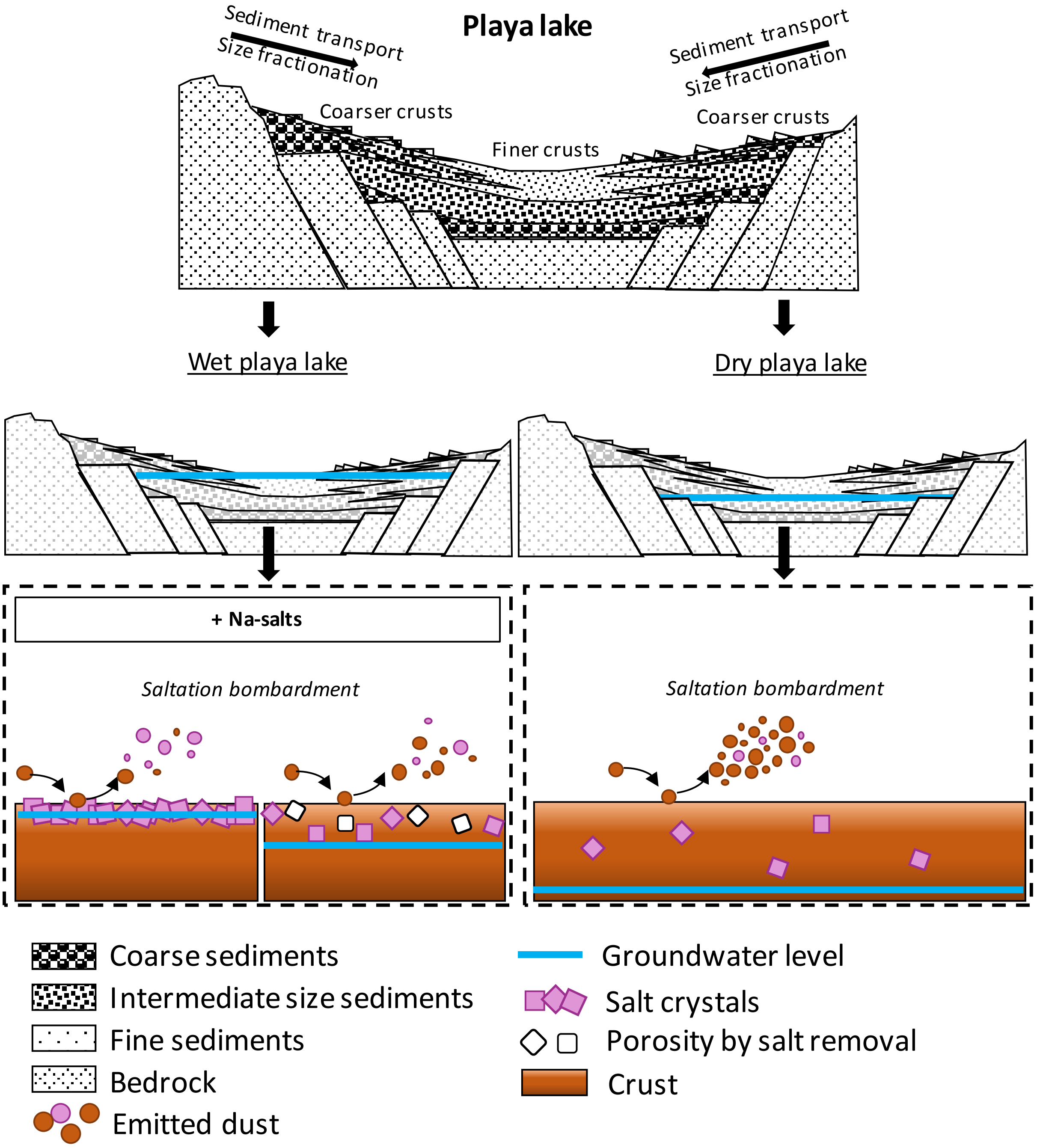
Playa lake
Sediment transport
Size fractionation
Sediment transport
Size fractionation
Coarser crusts
Finer crusts
Coarser crusts
Wet playa lake
Dry playa lake
+ Na-salts
Saltation bombardment
Saltation bombardment
Coarse sediments
Intermediate size sediments
Fine sediments
Bedrock
Emitted dust
Groundwater level
Salt crystals
Porosity by salt removal
Crust

Table 1. Full range (<2000 µm), <63µm and >63 to 2000 µm mean diameter, standard deviation, min., and max for minimally dispersed particle size distribution (MDPSD) and fully dispersed particle size distribution (FDPSD).

Surface	Location	N	**MDPSD**		
			Full range	≤ 63 µm	>63 to 2000 µm
			Mean of medians ± Std. Dev. [Min,Max]		
Crusts	Mojave	35	92 ± 74 [10,349]	22 ± 6.4 [11,34]	254 ± 71 [155,489]
Ripples		20	226 ± 88 [88, 418]	37 ± 6.0 [20,46]	276 ± 80 [130,424]
Crusts	Soda	17	63 ± 47 [10,156]	21 ± 6.5 [11,31]	234 ± 82 [155,489]
	Cronese	9	109 ± 60 [35,195]	18 ± 2.2 [15,22]	280 ± 40 [238,357]
	Mesquite	7	141 ± 117 [31,349]	28 ± 5.6 [21,34]	257 ± 79 [157,387]
	Ivanpah	1	35 ± NA [35,35]	16 ± NA [16,16]	314 ± NA [314,314]
	Coyote	1	101 ± NA [101,101]	20 ± NA [20,20]	254 ± NA [254,254]
Ripples	Soda	15	231 ± 87 [88,418]	39 ± 3.5 [29,43]	275 ± 77 [130,424]
	Cronese	2	264 ± 147 [160,368]	40 ± 8.8 [34,46]	292 ± 120 [208,377]
	Mesquite	2	167 ± 112 [110,225]	26 ± 8.9 [20,32]	286 ± 146 [183,389]
	Ivanpah	0	NA	NA	NA
	Coyote	1	179 ± NA [179,179]	32 ± NA [32,32]	236 ± NA [236,236]
Surface	Location	N	**FDPSD**		
			Full range	≤ 63 µm	>63 to 2000 µm
			Mean of medians ± Std. Dev. [Min,Max]		
Crusts	Mojave	35	37 ± 48 [4.9,240]	18 ± 6.6 [8.4,35]	306 ± 237 [106,1093]
Ripples		20	213 ± 92 [28,362]	29 ± 8.3 [15,48]	335 ± 99 [213,561]
Crusts	Soda	17	52 ± 61 [8.4,240]	19 ± 5.3 [12,27]	321 ± 212 [113,815]
	Cronese	9	17 ± 23 [4.9,77]	12 ± 3.1 [8.4,19]	381 ± 345 [144,1093]
	Mesquite	7	34 ± 28 [11,91]	24 ± 7.7 [16,35]	185 ± 104 [106,336]
	Ivanpah	1	12 ± NA [21,21]	15 ± NA [15,15]	347 ± NA [347,347]
	Coyote	1	8.4 ± NA [8.4,8.4]	12 ± NA [12,12]	187 ± NA [187,187]
Ripples	Soda	15	234 ± 82 [92,362]	31 ± 7.9 [21,48]	346 ± 97 [238,561]
	Cronese	2	236 ± 126 [147,325]	18 ± NA [18,18]	295 ± 108 [219,371]
	Mesquite	2	67 ± 56 [28,107]	27 ± 3.5 [24,29]	336 ± 173 [213,458]
	Ivanpah	0	NA	NA	NA
	Coyote	1	156 ± NA [156,156]	15 ± NA [15,15]	245 ± NA [245,245]

Table 2. Average and standard deviations of the mineral contents (wt %) from crust and aeolian ripple samples from the Mojave Desert and the different study basins. NaN, not a number. Maghemite is considered as Maghemite and Magnetite

	Clays	**Carbonate**	**Salts**	**Zeolites**	**Maghemite**	**Quartz**	**Feldspars**	**Gypsum**	**Amphibole**
CRUSTS	24±11	6.6±6.6	7.3±13	1.2±1.9	0.92±0.59	16±7.2	37±9.7	3.1±14	4.1±1.5
Soda	22±11	3.6±2.6	8.9±17	0.77±1.1	0.97±0.66	18±7.7	40±6.7	0.29±0.68	4.5±1.6
Cronese	31±11	5.4±1.8	2.2±3.4	2.4±1.7	1.0±0.28	14±7.3	40±5.5	<0.1	3.4±1.5
Coyote	28	7,2	1,2	8,5	0,48	11	37	<0.1	5.6
Ivanpah	36	6.9	<0.1	<0.1	1,2	15	36	<0.1	3.5
Mesquite	17±8.2	15±11	12±14	<0.1	0.71±0.75	14±5.8	24±12	15±29	2.8±1.4
RIPPLES	7.8±2.3	1.1±2.2	1.1±3,7	0.12±0.52	0.49±0.28	32±9.5	48±13	4.7±20	4.1±1.6
Soda	7.4±1.8	0.47±0.73	0.19±0.46	<0.1	0.49±0.25	35±4.5	52±4.7	<0.1	4.3±1.5
Cronese	8.4±0.60	1.2±1.7	<0.1	<0.1	0.83±0.33	32±9.0	53±0.03	<0.1	4.7±3.2
Coyote	7.9	2.3	<0.1	2,3	0.60	28	52	<0.1	3.5
Ivanpah	NaN	NaN	NaN	NaN	NaN	NaN	NaN	NaN	NaN
Mesquite	10±6.1	4.8±6.8	9.4±9.9	<0.1	0.19±0.27	10±14	15±21	47±60	3.7±1.5

Table 3. Fe content in wt % for total Fe (FeT) content, and in % for ascorbate Fe (FeA), dithionite (FeD), oxalate Fe (FeM) and structural Fe (FeS). NaN not a number.

	FeT	FeA %	FeD %	FeM %	FeS %
CRUSTS	3.0±1.3	1.8±0.92	17±7.2	2.1±1.2	79±8.5
Soda	3.1±1.2	1.5±0.81	14±2.5	1.5±0.49	83±2.8
Cronese	3.7±1.2	2.4±0.99	21±11	2.3±1.1	74±13
Coyote	3.5	1.8	14	2.4	82
Ivanpah	4.9	1.4	29	0.82	68
Mesquite	1.6±0.53	1.8±0.93	20±2.7	3.7±1.2	74±3.5
RIPPLES	1.9±1.1	1.4±1.2	12±5.6	2.4±1.8	84±7.5
Soda	2.0±1.2	0.98±0.39	10±3.4	2.1±1.8	87±4.4
Cronese	2.3±1.5	1.4±0.35	14±9.3	2.8±2.9	82±12
Coyote	1.3	3.4	26	3.0	68
Ivanpah	NaN	NaN	NaN	NaN	NaN
Mesquite	1.0±1.1	3.6±3.0	20±1.2	4.4±1.2	73±4.1

Table 4. Summarise MDPSD (µm), FDPSD (µm) median particle diameter, Quartz (Qtz, wt %), feldspars (Feld., wt %), clay mineral (Clay, wt %), carbonates (Carb., wt %), Na-salts (Na-S, wt %), Gypsum (Gp, wt %), total Fe content (FeT, wt %), exchangeable Fe (FeA, wt %), dithionite Fe (Hematite and Goethite, wt %), oxalate Fe (FeM, wt %) and structural Fe (FeS, wt %) for Mojave and Morocco crusts and Iceland top sediments. NaN not a number.

	MDPSD d(0.5)	FDPSD d(0.5)	Qtz	Feld.	Clay	Carb.	Na-S	Gp	FeT	FeA	FeD	FeM	FeS
Mojave	92	37	16	37	24	6.6	7.3	3.1	3.0	0.06	0.53	0.06	2.4
Morocco	113	37	48	9.4	17	22	7.0	0.64	3.6	0.07	1.1	NaN	2.4
Iceland	55	56	0.21	20	NaN	NaN	NaN	NaN	9.3	0.15	0.43	1.4	7.3